

Modelling of PV-Electrolyzer system for optimum operation

Analyzing the effect of varying irradiance, module parameters
and comparison of various configurations for best efficiency

N. R. Shriyan



Modelling of PV-Electrolyzer system for optimum operation

Analyzing the effect of varying irradiance,
module parameters
and comparison of various configurations for
best efficiency

by

N. R. Shriyan

for the Master Thesis

at the Shell International Solutions BV, Amsterdam.

to be defended publicly on Friday, August 21, 2020 at 10:00 AM.

Student number: 4786076
Project duration: Dec 20, 2020 – August 21, 2020
Thesis Committee: Prof. dr. Olindo Isabella, TU Delft.
Prof. dr. Marjan Popov, TU Delft.
Prof. dr. Hesam Ziar, TU Delft.
Dr. Zameer Ahmad, TU Delft.
Dr. Cor Van Kruijsdijk, Shell Global Solutions International B.V.

Cover image courtesy : DmytroPerov | Shutterstock

An electronic version of this thesis is available at <http://repository.tudelft.nl/>.



Summary

With emphasis on finding storage solutions for renewable based power plants, hydrogen has emerged as one of the prominent options. Hydrogen required in fertilizer, oil and gas industries etc., is produced using fossil fuels which emits carbon di-oxide 10 times the produced hydrogen. It is important to produce the hydrogen from green energy sources for this industrial use or storage use. Solar energy harvested from Photo-Voltaic (PV) technology can be used to produce hydrogen in an alkaline electrolyzer. Both PV and alkaline had a decent learning curve over past decades individually, but very less has been investigated or implemented on connecting it at large MW scale. Directly coupling the PV and electrolyzer systems will have least components contributing to inefficiencies, complexities etc. Additionally, the use of power converters and transmission devices would contribute to additional costs too. But in directly coupled systems there is no external control over the operating point of the system. Therefore, it is important to design the configuration in a way to have highest output.

In this study, a tool was made using MATLAB-Simulink, to optimize the PV-Electrolyzer directly coupled system. In literature many authors have done the same but none of them have included variation in space irradiance over PV farm, variation in PV module parameters due to manufacturing defects or defects arising over the period of use. These variations affect the IV curve of PV modules and in turn affect the performance of the whole system. Performance in this study was gauged using coupling efficiency, that is the power harvested from the system with respect to the total available maximum power from the PV plant. It was observed that after optimizing, the coupling efficiency in the range of 90-95% could be achieved in directly coupled systems. This was even with the variation upto 20% in parameters like irradiance and PV module parameters. If the best configuration is not available in the market, then the next best configuration is available as output of simulation. Even with variation of 10%, the maximum difference between the global maximum and other local maximums in the results is 3%. This 3% compromise results in energy loss of 870kWh and 148 euros loss per year for a 50kWp system. Which is 2.96 Euros/kWp loss, at 1 GW scale it may result into a loss of 2.96 million Euros, if we ignore the variations.

In comparison to the DC-AC-DC configuration that comprises of inverter, rectifier and transformer, the directly coupled system performed better. The efficiency was almost 5-10% more for directly coupled system in comparison to DC-AC-DC system. The weighted efficiency for both the configurations were calculated, where the weights were based on the occurrences and the energy contribution of an irradiance bracket. The weighted efficiency for directly coupled system was 95.7% and for DC-AC-DC was 90.63% for Amsterdam.

Acknowledgements

I chose to pursue my masters in Sustainable Energy Technology at TU Delft, after being motivated by the purpose of contributing towards a sustainable future of the energy systems. Over the period of 24 months, I have learned new things and honed many skills.

In the search for a suitable master thesis, my supervisor at TU Delft Dr.Olindo Isabella referred me to Dr.Cor van Kruijsdijk from Shell. I would like to thank both of them for granting me an opportunity to work on this interesting topic. Cor was always available to guide me. It was a privilege to work alongside him. He helped me settle down quickly in the organization. I would also like to thank my colleagues at Shell for supporting me through out this journey. It was unfortunate that we couldn't meet more in person due to the Covid lockdown.

I would like to thank Professor Arno Smets, Miro Zeman, Rene van Swaaij and Olindo Isabella, who helped me build my basic and applied knowledge of Photovoltaics through their amazing coursework. During my thesis of 9 months, Dr.Hesan Ziar and Dr. Zameer Ahmad have been helping me on a regular basis. Even with current covid situation, they have always been there virtually for my support. A big thanks to Parinita, Soham, Agney, Rishi, Vishwa, Omkar, Gopan and all friends who have been a part of this fun ride with me.

Finally I would like to thank my parents who have been very supportive with my career decisions.

Nikhil Shriyan
Amsterdam, August 2020

Contents

Summary	iii
Acknowledgements	v
List of Figures	x
Abbreviation	xii
Nomenclature	xiii
1 About the project	1
1.1 Overview	1
1.2 Existing work on green hydrogen	3
1.3 Research objectives	4
1.4 Report outline	5
2 Electrolyzer - A brief overview	6
2.1 Basic structure and operation of electrolyzers	6
2.1.1 Basic structure and operation of PEM electrolyzer	6
2.1.2 Overview of Solid-Oxide electrolyzer	7
2.1.3 Basic structure and operation of Alkaline electrolyzer	7
2.2 Alkaline electrolyzer setup at STCA, Amsterdam	9
2.3 IV curve characteristics of Alkaline electrolyzer	11
2.3.1 Effect on IV curves with varying cell parameters	14
3 Photo-voltaic systems	18
3.1 Single diode model	19
3.1.1 Five parameter model	20
3.2 Effects of varying irradiance on IV curve	21
3.3 Effects of varying temperature on IV curve	22
3.4 Effects of variability of module parameters	22
4 Working of direct coupling PV - Electrolyzer system	23
4.0.1 Directly coupled configuration	23
4.1 Literature review of PV-Electrolyzer systems	24
4.1.1 Literature review of direct coupling systems	25
4.1.2 PV-Electrolyzer systems with additional components	28
4.2 System configuration and simulation results of the STCA setup	29
4.2.1 Understanding the irradiance and module temperature to be measured	29
4.2.2 Weather station installation at STCA, Amsterdam	32
4.2.3 Current setup of PV modules and Electrolyzer stack	34
5 Understanding the tool developed	39
5.1 Self-programmed tool	39
5.1.1 Constraints for the simulation	39
5.1.2 Logic for optimization	40
5.1.3 Inclusion of ohmic losses	43

5.2	Results for directly coupled system	44
5.2.1	Performance of directly coupled system with time varying irradiance	44
5.2.2	Change in coupling efficiency with inclusion of space varying irradiance	46
5.2.3	Variation in coupling efficiency with months	50
6	Power converters & transformers in DC-AC-DC configuration	52
6.1	Varying DC-AC-DC configuration efficiency	53
6.1.1	Efficiency variation of inverters	53
6.1.2	Efficiency variation of transformers.	54
6.2	Comparison of DC-AC-DC and direct coupling configuration	56
6.2.1	Weighted efficiencies of directly coupled and DC-AC-DC configurations.	56
7	Conclusion	58
7.1	Recommendations	59
	Bibliography	62
A	Appendix	63
A.1	PV module characteristic	63
A.2	Electrolyzer characteristics	64
A.3	Inverter characteristics	64

List of Figures

1.1	Fossil Fuel to Renewable	1
1.2	Global Hydrogen Demand, (IRENA, 2019)	2
1.3	Solar Hydrogen demonstration project in Neunburg, Germany, Schucan (2000)	3
1.4	PV-panels on house roof and minivan ,Schucan (2000)	4
2.1	PEM Electrolyzer, (Carmo et al., 2013)	7
2.2	Working of Alkaline Electrolyzer, (Regine Reissner, 2015)	8
2.3	Unipolar Alkaline Electrolyzer, (Ibrahim Dincer, 2018)	9
2.4	Bipolar Alkaline Electrolyzer, (Ibrahim Dincer, 2018)	10
2.5	Alkaline Electrolyzer from Hydrogenics	10
2.6	Polarization Curve, (Yakdehige, 2017)	11
2.7	Electrolyzer IV Curve with varying Temperature, (Martin, 2020)	13
2.8	Hydrogen Temperature variation with Irradiance for 26-06-2019	13
2.9	Hydrogen Temperature variation with Irradiance for 28-06-2019	14
2.10	Selected IV curve for STCA electrolyzer	14
2.11	Effect of Varying Active Cell area	15
2.12	Effect of Varying number of cells	16
2.13	Effect of Varying Active Cell area and number of cells together	16
3.1	Global PV potential SOLARGIS (2020)	18
3.2	One Diode Model- electrical circuit equivalent of solar cell (Sandia National Laboratories, 2018)	19
3.3	IV curve of PV module	20
3.4	Variation of IV with varying Rsh, Rs	21
3.5	IV graph varying with Irradiance and Temperature	21
3.6	Stepped IV curve	22
4.1	Directly Coupled System	23
4.2	Operating Points of Directly Coupled Systems	24
4.3	MPP region for 2 years, (García-Valverde et al., 2011)	25
4.4	Maeda et al. (2016) Setup	27
4.5	H ₂ production in the 6 cities (Sayedine et al., 2016)	27
4.6	Number of start-stops for electrolyzer with PV integration and wind integration, (Ursúa et al., 2016)	28
4.7	Components of Global Horizontal Irradiance, (Jeffrey R. S. Brownson, 2020)	30
4.8	Different solar angles, (Rosa-Clot and Tina, 2017)	30
4.9	Equipment Placement	33
4.10	Sunshinometer from EKO Istruments	33
4.11	DNI peaks in 15 secs, ((Pó et al., 2018))	34
4.12	PV-Electrolyzer set-up at STCA, Amsterdam	34
4.13	STCA Rooftop Installation	35
4.14	IV curves of PV and Electrolyzer	35
4.15	Variation in Irradiance and module parameters	36

4.16	Heatmap of Coupling Efficiency with variation in Irradiance	37
4.17	Histogram of yearly irradiance and energy produced in MWh	37
5.1	PV Simulink Model	41
5.2	Electrolyzer IV curve's constraints	41
5.3	Logic for simulation	42
5.4	All possible IV curves for the 50kW system	43
5.5	Simple layout of directly coupled system	44
5.6	Daily Irradiance Profile, (Balafas et al., 2010)	45
5.7	IV curves of all possible configurations	46
5.8	Closeup of all IV curves	47
5.9	Deviation in Coupling Efficiency	47
5.10	IV curves of all possible configurations with 5% variation	48
5.11	Difference in Coupling Efficiency with 5% variation	48
5.12	Without considering the ohmic loss	48
5.13	IV curves of all possible configurations with 10% variation	49
5.14	Difference in Coupling Efficiency with 15% variation	50
5.15	Effect of adding ohmic losses	50
5.16	Heatmap showing the effects of including ohmic losses	50
5.17	Month wise variation in efficiency	51
6.1	DC-AC-DC configuration	52
6.2	Varying inverter efficiency	53
6.3	Transformer	54
6.4	Varying efficiency of transformer	55
6.5	Efficiencies of each component	55
6.6	Comparison of varying efficiency between directly coupled and DC-AC-DC	56
6.7	Occurrences of each irradiance bracket at STCA in 2019-2020	57
A.1	Electrical Data of Module	63
A.2	Mechanical data and Temperature Characteristics	63
A.3	Electrolyzer datasheet	64
A.4	Coefficients of CEC model for Inverter	64

Abbreviation

AST	Apparent Solar Time
KNMI	Koninklijke Nederlands Meteorologisch Instituut
MPPT	Maximum Power Point Tracking
PEM	Proton Exchange Membrane
PV	Photovoltaic
STC	Standard Test conditions
STCA	Shell Technology Center Amsterdam

Nomenclature

α	Solar altitude	[°]
γ	Module azimuth	[°]
ψ	Persistence	
θ_z	Solar azimuth	[°]
AOI	Angle of Incidence	[°]
I_{mpp}	Current at maximum power point	[A]
I_{sc}	Short circuit current	[A]
K_t	Daily clearness index	
k_t	Clearness index	
n	Ideality factor	
N_p	PV modules in parallel	
N_s	PV modules in series	
P_{aco}	Maximum AC power at reference conditions	[W]
P_{ac}	AC power output	[W]
P_{dco}	DC power at reference conditions	[W]
P_{dc}	DC power output	[W]
P_{mpp}	Maximum power point	[W _p]
R_{sh}	Shunt resistance	[ohm]
R_s	Series resistance	[ohm]
V_{dco}	DC voltage at reference conditions	[V]
V_{dc}	DC input voltage	[V]
V_{mpp}	Voltage at maximum power point	[V]
V_{oc}	Open circuit voltage	[V]

1

About the project

1.1. Overview

According to a survey by Business Insider, 48.8% of participating millennial felt climate change is the biggest problem in today's world (Loudenback and Jackson, 2018). A research by Cook et al. (2013), suggests that around 97% of climate researchers acknowledge climate change as anthropogenic (i.e. caused by humans). The carbon dioxide emissions from various sectors which fulfills the ever increasing demands of humans, has been the prime reason for climate change. Out of all the sectors, the power production sector gives out the highest amount of carbon emissions worldwide which is 13603 MT (IEA, 2020b). The fossil fuel dominated power sector needs to be replaced by green energy producing renewable energy plants as shown in figure 1.1.

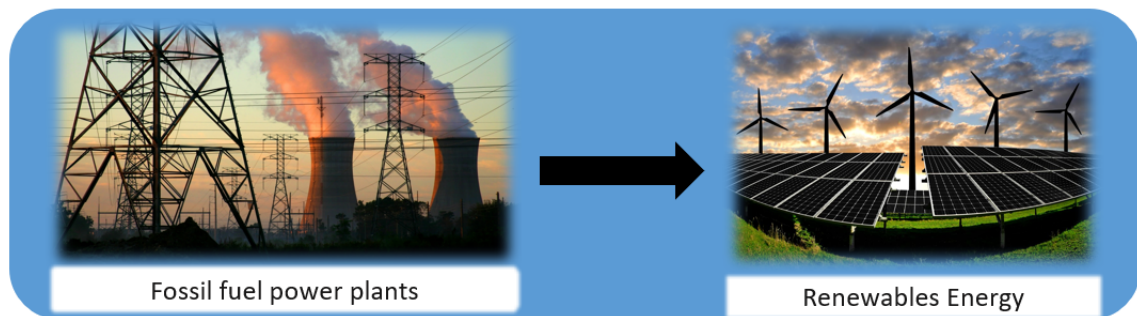


Figure 1.1: Fossil Fuel to Renewable

The oil crisis of 1970's was one of the major factor why people started looking for alternative energy sources. Huge technological advancement in renewable energy technologies has taken place over past 3-4 decades through intensive research and diffusion of technologies in niche markets. Through huge manufacturing boost and deployment of solar, the Capex has come down considerably. In the past 5 years, PV auction prices have dropped by roughly 100 USD/MWh (IEA, 2020a). But the intermittent nature of renewable energy makes it dependant on storage technologies for steady supply of power. Unlike renewable energy technologies, storage comparatively has still remained more expensive. Green hydrogen produced using renewable energy is considered to be one of the prominent option for energy storage and grid stabilization. Recovering energy from stored hydrogen through fuel cells has been done for decades by NASA using fuel cells.

There are mainly 3 variety of hydrogen produced, namely green hydrogen, blue hydrogen and grey hydrogen. Green hydrogen is produced from renewable energy, grey hydrogen is produced using natural gas and blue hydrogen is produced using natural gas too but with carbon capture technology (Industries, 2020). Every kg of grey hydrogen produced using natural gas leads to 10 kg of CO₂ (Peters, 2020). For blue hydrogen the additional cost of carbon capture and disposing of CO₂ is still a concern. Green hydrogen amongst them is the cleanest source of hydrogen with least emissions during the process of converting power to gas. This green hydrogen can store the excess energy from solar during peak irradiance period and supply energy back to the grid during the absence of solar energy.

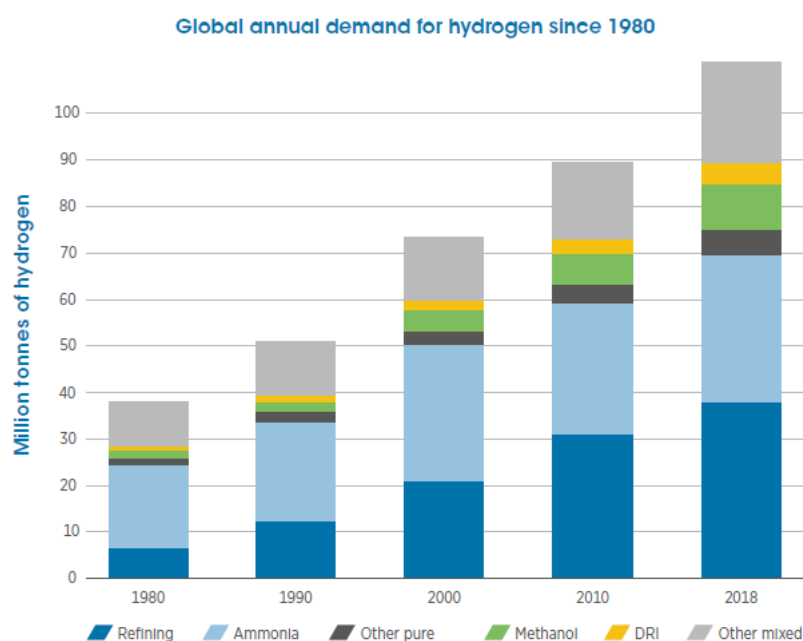


Figure 1.2: Global Hydrogen Demand, (IRENA, 2019)

Many of the industries like fertilizer producers, oil & gas etc require hydrogen for different processes. As shown in figure 1.2, over a 100 million tonnes of hydrogen is currently required by multiple industries (IRENA, 2019). Currently, 75% demand of hydrogen in oil & gas sector is catered by production of hydrogen by burning methane (Europe, 2020). Feasibility of using hydrogen instead of coal/natural gas in steel plants is still being implemented at pilot level projects. Thus, green hydrogen as a fuel will be essential in helping the decarbonization of industries and as well as for storage of energy. But it is essential that this hydrogen comes from a clean source i.e. producing it with the renewable energy. Latest EU hydrogen strategy of European Commission is aiming to boost the green hydrogen production from renewables. EU targets 40GW of renewable hydrogen electrolyzers deployment by the end of 2030 (Commission, 2020). Even worldwide countries are supporting the development of hydrogen use for decarbonizing the industries. Netherlands is planning to use 3-4GW wind energy for hydrogen production from North Sea by 2030, which may go upto 10GW by 2040. Shell and Gasunie are partnering for this project (de Laat, 2020). Similarly, Australia is eyeing development of solar and wind energy upto 15 GW scale for hydrogen production (IRENA, 2019). These conditions have motivated the green hydrogen research

lobby worldwide.

To increase the share of green hydrogen from renewables, it is necessary to optimize the production from the available options. Major factor that dissuades industries from using green hydrogen is the cost. But with ever decreasing cost of solar, wind power, etc., it is now possible to make green hydrogen cheaper with proper optimization during its production. PV farm directly coupled with electrolyzer with least amount of power electronics involved can be seen as a solution with lower cost. Before investing into any technology, the investor must be convinced by the bank-ability of the technology. A proper tool for selecting the configuration and understanding the varying factors affecting the pv-electrolyzer direct coupling, is one of the important steps towards the bank-ability of this system.

1.2. Existing work on green hydrogen

Production of hydrogen using electrolysis was introduced to the world in 1789 by Adriaan Paets van Troostwijk and his friend Johan Rudolph Deiman from The Netherlands. Russian engineer Dmitry Lachinov introduced a method for industrial synthesis of hydrogen using electrolyzer in 1884 (Chisholm and Cronin, 2016). Similarly, concept of green hydrogen production is not very new, rather it is almost a century old. In 1927, Nel (2019) first installed a small scale electrolyzer coupled to hydropower in Notodden, Norway to test the production of green hydrogen for fertilizer production. By 1929, Nel had installed 440 electrolyzers exceeding $60,000 \text{ Nm}^3/\text{h}$ at Rjukan, Norway (Nel, 2019).



(a) Birdview of Neunberg Plant



(b) Electrolyzers

Figure 1.3: Solar Hydrogen demonstration project in Neunburg, Germany, Schucan (2000)

In the area of green hydrogen production from solar energy the research and pilot projects have been going on for decades. Figure 1.3a and 1.3b, the solar hydrogen demonstration project in Neunburg, Germany that had collected the operation data for 10 years from 1986 to 1997. This project required the grid to balance the system, that is why all the hydrogen produced is not green. The project started with initial struggles in getting the safety part right and understanding the risks associated with various systems involved. After initial few turbulent years especially due to the use of all prototype systems, it showed the possibility of safe operations of all electrolyzer prototypes (200kW), PV modules, etc., over this period (Szyszka, 1998).

In 1991, a very rare private investment by an individual named Markus Friedli was done for installing a PV powered electrolyzer was installed at his residence in Switzerland as



Figure 1.4: PV-panels on house roof and minivan ,Schucan (2000)

shown in figure 1.4. This system was also balanced using a grid connection and a battery. Data from literature showed it had performed without a glitch for a period of at least 7 years. PHOEBUS demonstration project in Jülich, Germany had demonstrated a PV-alkaline electrolyzer system with battery and a fuel cell load in 1997. A common DC-bus was used to connect all the systems and ran it independent from the grid. 10 major pilot studies for solar-electrolyzer PV coupling like these were already done in kW scale during 1990's as reported by Schucan (2000) in 1999. These studies have shown safe and possible operation of directly coupled solar and electrolyzer operations upto 10 years. Some of these studies would be discussed in detail in section 4.1.2.

Lately, in the past decade the research in solar hydrogen has rekindled amongst the researchers. Now there has been a constant effort to optimize the PV-Electrolyzer coupling, i.e. to maximize the energy from PV and to deliver it into the electrolyzer with least losses possible. With clear advantage in terms of CAPEX cost, direct coupling of PV-electrolyzer system has been the most researched and preferred configuration even for pilot projects. Researchers like Rahim et al. (2015), Sayedin et al. (2016), Duc et al. (2019), Maeda et al. (2016), García-Valverde et al. (2011), Kovač et al. (2019) and Paul (2009), have done research on PV-Electrolyzer direct coupling. Outcomes from these researches would be later discussed in section 4.1 with more emphasis. A general outcome from this literature review was that the optimization was done either using single PV module or variation of irradiance was considered only with respect to time in case of kW scale system. In this thesis project, optimization would be done for a 50kW system and effect of both space & time varying irradiance would be considered. The aim of this project would be to develop a tool, which helps in understanding the best configuration for directly coupled PV-electrolyzer system and other varying factors affecting it. Data from physical setup of PV-Electrolyzer system at Shell Technology Centre Amsterdam would be used.

1.3. Research objectives

- To set constraints while designing a directly coupled PV-electrolyzer system.
- Developing a tool to do an exhaustive search for all possible configurations within the defined boundaries. (By configuration it means the series-parallel arrangement of PV

- modules and the number of electrolyzer cells in series inside an electrolyzer stack.)
- Understanding the impacts of irradiance varying in time and space on the coupling efficiency.
 - To gauge the effects of module parameter variation on coupling efficiency.
 - Observing the seasonal variation's affect on different configuration.
 - Comparing the efficiency of directly coupled system with a system connected with power converters in DC-AC-DC system.

1.4. Report outline

The first chapter 'About the project' gave a brief overview of why this project was initiated, history and the current update on related researches and what are the research objectives for this thesis project. The second chapter 'Electrolyzer - A Brief Overview', explains in detail about the working principles of alkaline electrolyzers, explains the current installed electrolyzer setup at Shell Technology Center Amsterdam (STCA) and the effects of different variables on the IV curve of electrolyzers. In the third chapter 'Photo-voltaic Systems', it would be explained how the IV curve of PV system was obtained and how it would be affected by various factors. Then the crux of this study, working of directly coupled PV-electrolyzer system would be explained in chapter 4, also the literature pertaining to it. The tool developed to optimize this configuration and its results would be explained in chapter 5. Sixth chapter introduces the second configuration of DC-AC-DC system and its varying efficiencies with varying load. In sixth chapter both the configurations would be compared and their weighted efficiencies would be calculated. Finally chapter 7 concludes this study with some recommendations for future research.

2

Electrolyzer - A brief overview

In this chapter, types of electrolyzers and their working will be explained. Each of their characteristics, advantages and disadvantages are weighed against each other in section 2.1. The evolution of alkaline electrolyzer over past century and the basic structure & operation of alkaline electrolyzer is explained with special focus on the existing installed electrolyzer at Shell Technology Center Amsterdam (STCA) in section 2.1.3. Finally the chapter concludes with an explanation of the IV curve characteristics of alkaline electrolyzer in section 2.3.

2.1. Basic structure and operation of electrolyzers

After Adriaan Paetsvan Troostwijk and his friend Johan Rudolph Deiman from The Netherlands introduced the production of hydrogen using water electrolysis in 1789, the field of hydrogen as a fuel has come long way. Right from the use of hydrogen in fuel cells by NASA for power production inside space shuttles, now, hydrogen is poised to solve the intermittency problem of renewable energy. There are three major types of electrolyzer available for producing hydrogen, namely, Alkaline Water electrolyzer, Proton Exchange Membrane electrolyzer (PEM) and Solid-oxide electrolyzer. Each of them have their own distinct advantages and disadvantages.

2.1.1. Basic structure and operation of PEM electrolyzer

Proton Exchange Membrane electrolyzers also known as Polymer Electrolyte Membrane Electrolyzer was first introduced in 1960 by General Electric scientists Thomas Grubb and Leonard Niedrach. Usually Nafion is used for the membrane material, Platinum for cathode and Iridium for Anode in this type of electrolyzer. H^+ ions flows through the polymer membrane of PEM electrolyzer from anode to cathode. At cathode two H^+ ions gets combined with two electron to form Hydrogen as shown in figure 2.1. This type of electrolyzer works at 20-100°C range. Membrane allows proton and very low crossovers of gas even at high pressures (Carmo et al., 2013).

Starting with the pros for PEM electrolyzer, it has high power density of 4.4 W/cm². The upper limit of current density can go upto 2 A/cm². Main advantage of PEM is it can work under lower partial load range between 0-10% (Carmo et al., 2013). This advantage has rekindled the interests of researchers for the application of storage combined with ever

electrolyzer has got the biggest learning curve of almost a century experience in industries. Due to this very reason, lesser costs, and proven reliability, alkaline electrolyzers are still amongst the highest deployed electrolyzers. Even with limitations at lower partial load range, it is still trusted and tested for directly coupling with renewable technology.

Construction and working of Alkaline electrolyzers

Alkaline Electrolyzer consists of Nickel electrode immersed in KOH electrolyte with 25-30% concentration as shown in figure 2.2. A diaphragm typically separates the two electrodes, which allows the transfer of OH^- ions from cathode to anode while preventing the produced gas to crossover. DC power is supplied at the electrodes of the electrolyzer. A continuous feed of water is present on both the electrode sides. H^+ ions are reduced on cathode side to form hydrogen gas with the half cell reaction shown in equation 2.1. While OH^- ions travel to the anode side get oxidized forming water, oxygen gas and 2 electrons as shown in equation 2.2. The gas is produced on the face of electrode towards the diaphragm, but the gases escape through the porous electrodes towards the opposite of electrode. The gases produced are further sent into a separator. Hydrogen is purified further for impurities while the oxygen is let out.

The cathode side half-cell reaction is given as:



The anode side half-cell reaction is given as:

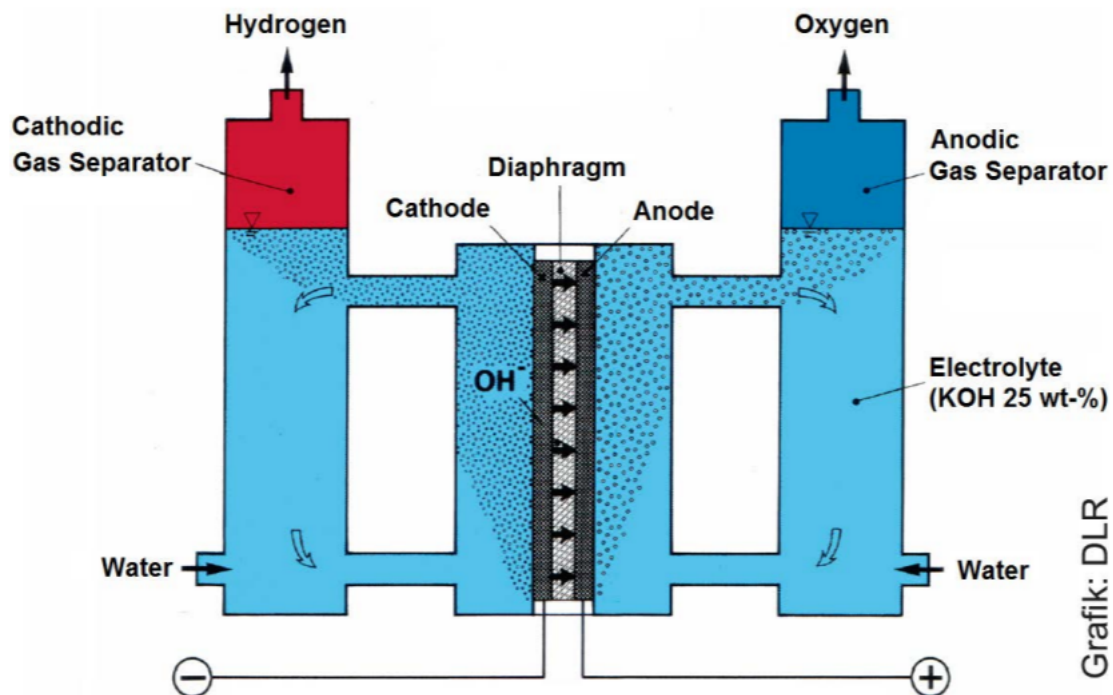


Figure 2.2: Working of Alkaline Electrolyzer, (Regine Reissner, 2015)

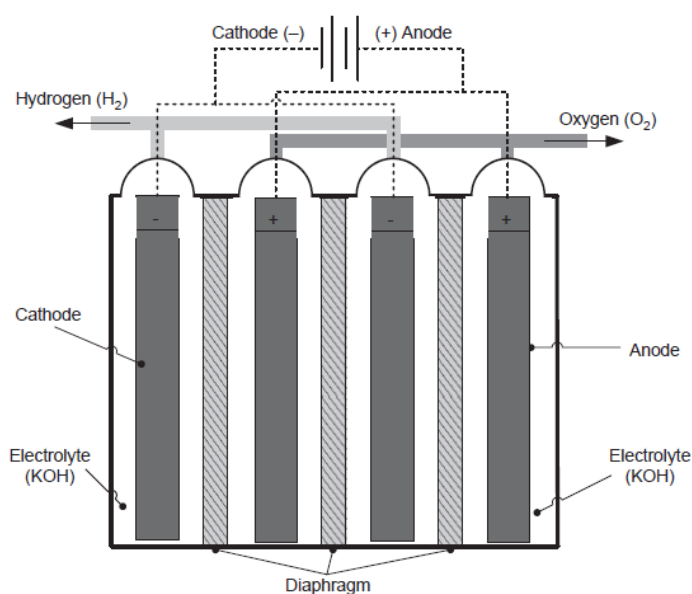


Figure 2.3: Unipolar Alkaline Electrolyzer, (Ibrahim Dincer, 2018)

Further the alkaline electrolyzers are divided into two categories namely bipolar and unipolar type, based on their electrode wiring type. In unipolar type, all the cells are connected in parallel thus the total voltage across the stack is the voltage across a single unit cell and the total current is the sum of current flowing through individual unit cells. Unipolar has simpler design and costwise is more effective. It also has some disadvantages like power requirement is on higher side and lower temperature limit. In bipolar type, all the cells are connected in series thus, the current flowing through the stack is the current flowing through one single unit cell and the voltage across the stack is sum of individual voltages of the unit cells in the stack (Regine Reissner, 2015), (Ibrahim Dincer, 2018). The current density in bipolar configuration is higher, even the pressure and operating temperature limit is higher than the unipolar configuration (Ibrahim Dincer, 2018). The construction of Bipolar and unipolar electrolyzer types are as shown in the figure 2.3 & figure 2.4.

2.2. Alkaline electrolyzer setup at STCA, Amsterdam

The electrolyzer setup at STCA, Amsterdam is shown in figure 2.5. The bipolar electrolyzer stack is at the bottom, which contains 60 cells in series and each with 1000cm^2 active area. The working at each individual cell was explained in section 2.1.3. The gases and electrolyte rises from the stack to the separator tank due to thermo-siphon effect. The electrolyte and the gas is separated in the gas separators. The electrolyte is cooled, maintained within the optimum operating temperature and fed back into the electrolyzer stack. The gases after the gas separator, moves into their respective coolers to knock out the water and keep it in safe temperature range. After which hydrogen is stored in tanks and oxygen is let out.

This electrolyzer can run on either grid connected or directly coupled PV modes, as per selection by the user. For the grid connected mode, the AC power is connected to the electrolyzer supply. The electrolyzer has an inbuilt rectifier for conversion to DC and its control to limit the maximum operating point on the electrolyzer IV curve within safe

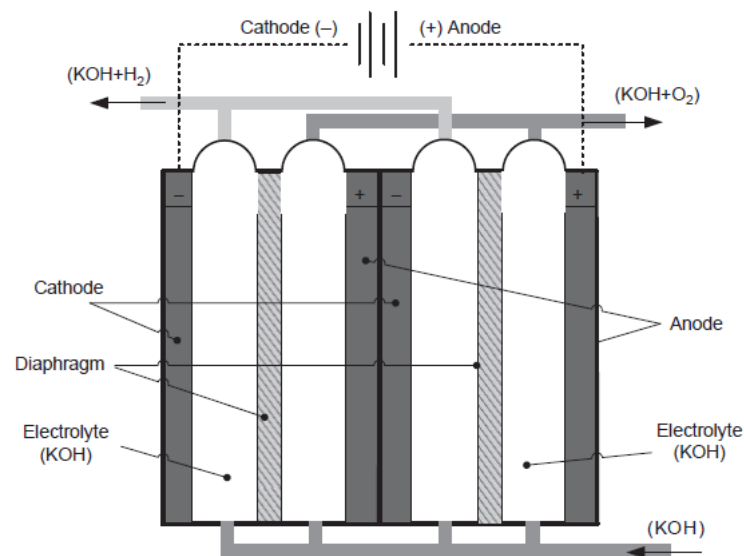


Figure 2.4: Bipolar Alkaline Electrolyzer, (Ibrahim Dincer, 2018)

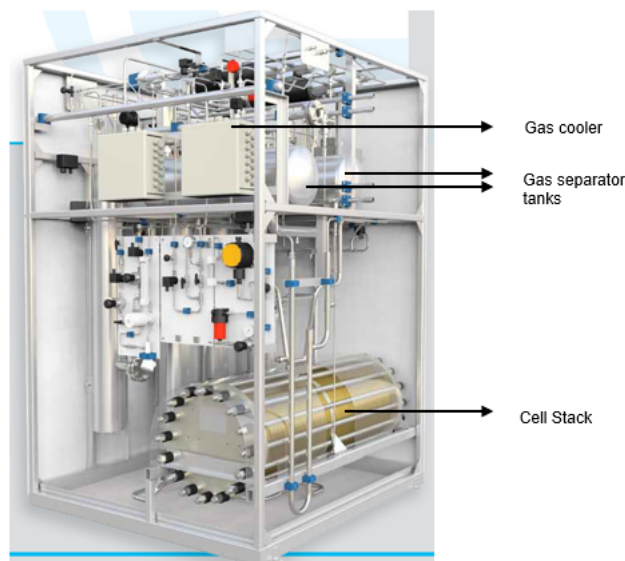


Figure 2.5: Alkaline Electrolyzer from Hydrogenics

operating limits. Electrolyzers have this upper limit beyond which the operations may cause damage to the electrolyzer, for this electrolyzer it is 120V and 450A on its IV curve in the temperature range of 60-65°C. A lower operating limit for electrolyzer is also set to avoid the excessive cross over of produced hydrogen gases at lower current density. At lower current density the oxygen produced is very low and the contamination of hydrogen in oxygen increases with decreasing current density (Schröder et al., 2004). Beyond the set lower limit of current density, the hydrogen contamination in oxygen has safety concerns and breaches the explosion limit. For the same reason this electrolyzer doesn't turn on till the 35% of its rated capacity is not reached.

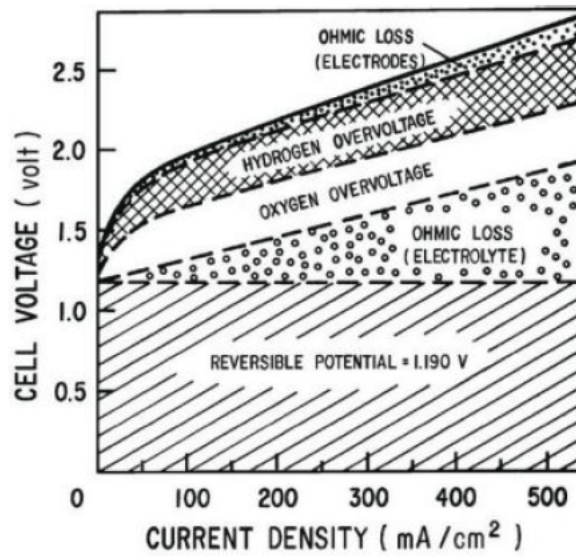


Figure 2.6: Polarization Curve, (Yakdehige, 2017)

2.3. IV curve characteristics of Alkaline electrolyzer

IV curve of alkaline electrolyzer also known as polarization curve is plot of cell voltage against the current density. The points on this polarization curve determines the operating points of this electrolyzer. The reversible voltage of cell determines the offset of this curve from the origin. Other factors affecting these curves are ohmic losses in electrolyte, ohmic losses in electrode, hydrogen over-voltage and oxygen over-voltage as shown in figure 2.6 (Yakdehige, 2017). Each of these components would be explained in detail below:

Reversible cell voltage

Reversible Voltage is the minimum voltage to be applied across the electrode to start the reaction. It depends on the Gibbs free energy required for water splitting. The standard Gibbs energy for splitting water is 237kJ/mol at standard conditions. The reversible cell voltage thus can be calculated as shown in equation 2.3. According to Faraday's Law:

$$U_{rev} = \frac{\Delta G}{z * F} \quad (2.3)$$

Where F is the Faraday's constant = 96485C/mol and z is electrons exchanged during the reaction (2 in this case). Thus at standard conditions $U_{rev} = 1.229V$, which changes with temperature and pressure. U_{rev} decrease slowly with temperature increase (Ulleberg, 2003).

Ohmic loss

The electrolyte, diaphragm, electrodes provides some resistance to the electron flow inside the cell, thus giving rise to ohmic losses in the electrolyzer cell. This loss is directly proportional to the current density in the electrolyzer cell. As seen in figure 2.6, the ohmic loss does increase towards the higher spectrum of current densities. This loss is also strongly related to temperature, with increase in temperature ohmic losses decreases. Ohmic losses is given by equation

$$U_{ohmic} = \frac{r_1 + r_2 T}{A} I \quad (2.4)$$

r_1, r_2 are coefficients related to electrolyte (Ulleberg, 2003).

Hydrogen and Oxygen activation overvoltage

Over voltage or activation over potential is the energy needed to transfer electrons from or to the electrodes at each end. It is highly dependant on the catalytic properties of the anode and cathode. This activation over is given by equation 2.6.

$$U_{act} = s \log\left(\frac{t_1 + \frac{t_2}{T} + \frac{t_3}{T^2}}{A} I + 1\right) \quad (2.5)$$

where t_1, t_2 and t_3 are the properties of electrodes. This activation voltage is inversely proportional to temperature.

Finally the complete IV curve characteristics equation for an electrolyzer cell can be summed up as following:

$$U = U_{rev} + \frac{r_1 + r_2 T}{A} I + s \log\left(\frac{t_1 + \frac{t_2}{T} + \frac{t_3}{T^2}}{A} I + 1\right) \quad (2.6)$$

A seven step procedure was mentioned by Ulleberg (2003) for calculating the 6 parameters of the electrolyzer IV curve. These parameters vary with each electrolyzer based on their electrodes and electrolyte. First, the experimental data for all operating points for various temperatures are plotted and r, s, t values can be found by curve fitting.

Effect of varying temperature

The performance of electrolyzer increases with its operating temperature. As can be seen from figure 2.7, the data from the STCA's electrolyzer suggests the same. The purple colored dots are operating points when hydrogen production temperature was between 65-70°C, which gives the steepest IV curve. With decreasing temperatures the slope decreases for the IV curve and thus the performance too. It is seen that blue dotted curves with least operating temperature range of 20-30°C is the lowest performing region. The part $(r_1 + r_2 T)/A$ in equation 2.6, represents the slope part of this IV curve, it can be clearly seen that this slope is directly proportional to the temperature.

In the figure 2.8, 2.9, the temperature of hydrogen and electrolyte becomes constant at 65°C, which controlled by the heat exchanger of electrolyte. The temperature measurement of hydrogen takes place at the exit point of electrolyzer from the stack, so it takes time to have a uniform temperature in 220L electrolyte. It can be seen in figure 2.8, it takes almost 2hrs for electrolyte temperature to reach 65°C and in figure 2.9, it takes 4hrs for the same. The difference in both scenarios being the starting temperatures which were 38°C and 21°C respectively, thus second case takes more time in reaching the equilibrium. The heat exchanger kicks in when temperature breaches 65°C and cools it back to the same temperature. The reason why heavy fluctuation of temperature between 65-68°C was seen due to the turning on and off of temperature control repeatedly.

In this study, the IV curve for temperature range 50-65°C was considered, as for the maximum period after achieving the 50-65°C equilibrium it remains constant in that range. The

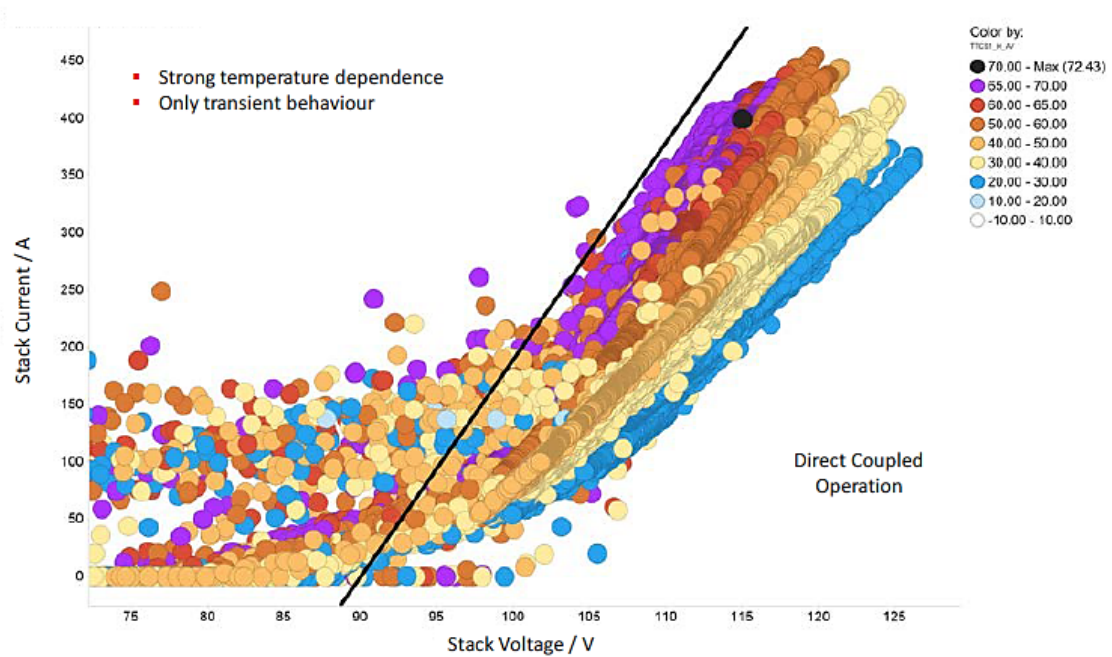


Figure 2.7: Electrolyzer IV Curve with varying Temperature, (Martin, 2020)

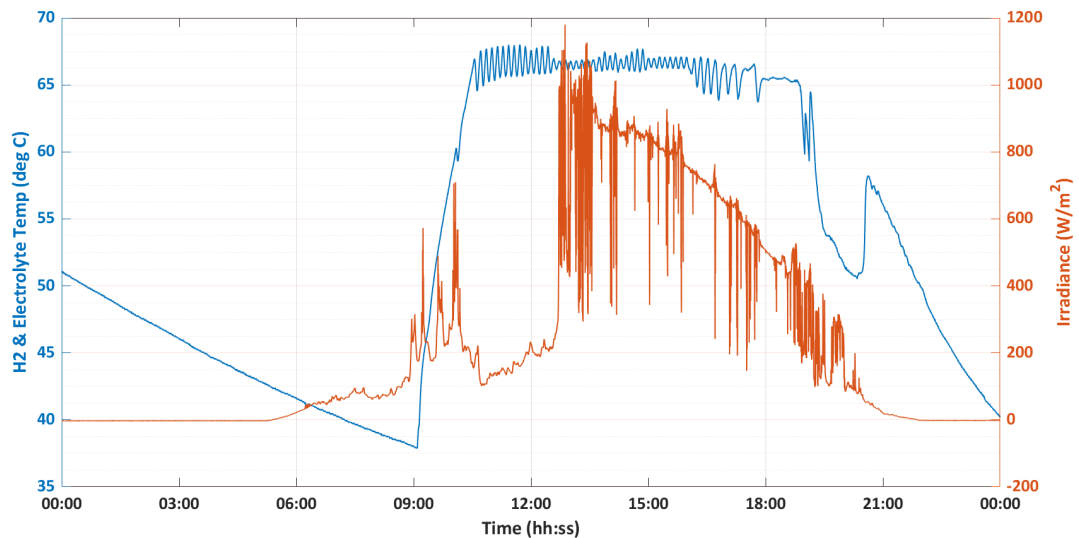


Figure 2.8: Hydrogen Temperature variation with Irradiance for 26-06-2019

temperature near electrolyte active cell area determines mainly the operating conditions of electrolyzer, which should be achieved by Ni electrodes in minutes rather than hours. As can be seen some blue dotted points in figure 2.7 under the region of 50-65°C. This is mainly due to the fact that the temperature near the electrode is already near the range of equilibrium unlike the electrolyte temperature near the measurement location. But a sophisticated electrolyzer model should be used to consider this temperature variation as well.

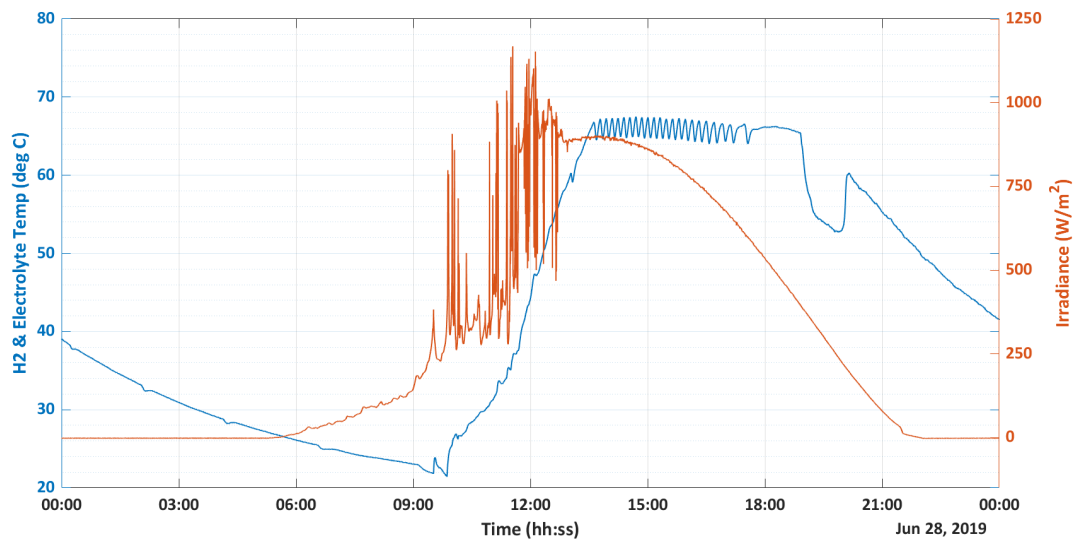


Figure 2.9: Hydrogen Temperature variation with Irradiance for 28-06-2019

2.3.1. Effect on IV curves with varying cell parameters

IV curves of electrolyzer can be varied by changing various cell parameters individually or in combination of all factors. Each of these parameters affect the IV curve in a different way. Parameters that mainly can affect the electrolyzer IV curves are:

- active cell area per cell
- number of cells in series in a electrolyzer stack
- number of cells in parallel in a electrolyzer stack

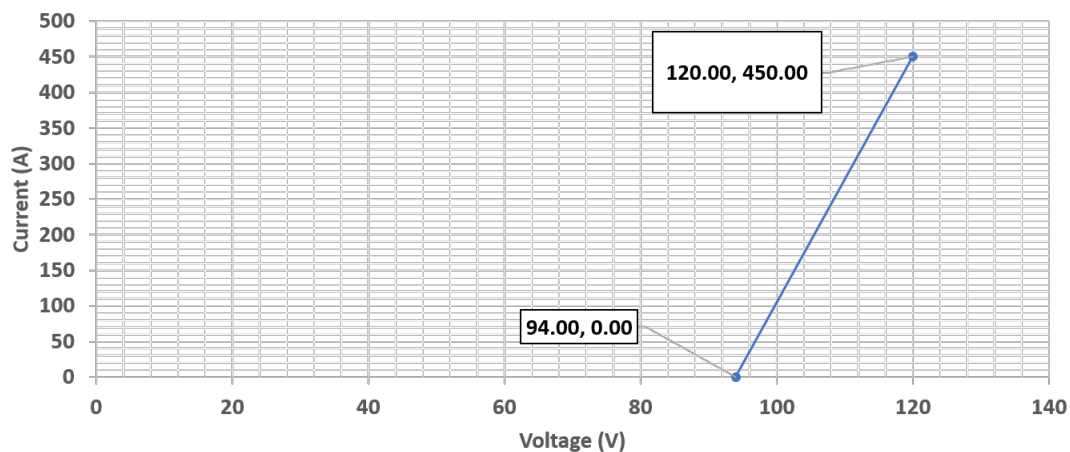


Figure 2.10: Selected IV curve for STCA electrolyzer

As explained in the previous section, the temperature for most part of time period remains constant in the range of 50-65°C, therefore straight line representing this region from figure 2.7 was picked. The constant slope line selected for the STCA's electrolyzer is shown in the figure 2.10. Also the initial logarithmic part of the IV curve was not considered as these lower current regions occur below the range of 250 W/m² and occurs for a short period

of timescale in microseconds compared to the minimum timescale for this study is hourly timescale . The equation of the straight line is given by:

$$V = 93.99 + 0.057I \quad (2.7)$$

From the electrolyzer data from STCA, it can be seen that the extrapolation of IV curve as a straight line intersects at 1.556V and maximum voltage per cell is 2V. The current density varies between 0 to 0.45mA/cm². These values and by the curve given in figure 2.10, various parameters of cell stack can be varied and new IV curves could be generated.

Effect of varying active cell area

As seen before, the IV curve for 60 cells, 1000cm² active area cell electrolyzer as shown in figure 2.10. Now, increase the per cell active area keeping the number of cells per stack constant at 60. This causes increase in need of current at same voltage, as the per cell current density remains the same. As can be seen in figure 2.11, the height of IV curve increases, that is, the peak current increases with increasing active cell area. The slope and magnitude of the line segment changes. It can be clearly seen that this causes increase in capacity of electrolyzer in terms of kW. Increasing the active area from 1000 to 1167 cm² will lead to increase of kW capacity from 54 kW to 63 kW.

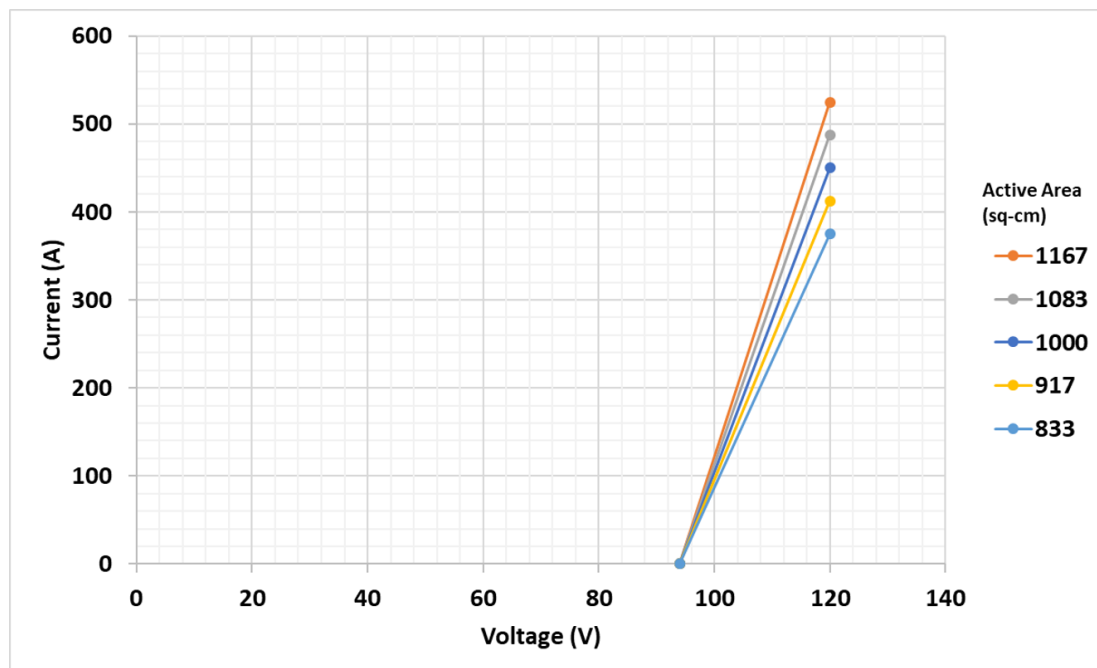


Figure 2.11: Effect of Varying Active Cell area

Effect of Varying number of cells

With increasing the number of cells in series in the stack of electrolyzer while keeping the active area per cell same the effect was observed as shown in figure 2.12. It could be seen that the slope of straight line remains constant but the voltage intercepts increase due to increased number of cells. The peak current remains the same as current density remains constant and the active area per cell was kept constant. Thus, due to same peak current

and increased peak voltage, it is seen that the kW capacity of the electrolyzer is increased while adding cells of same active area in the stack. The stack with 70 cells becomes 63kW as compared to the 54kW capacity of 60 cells stack.

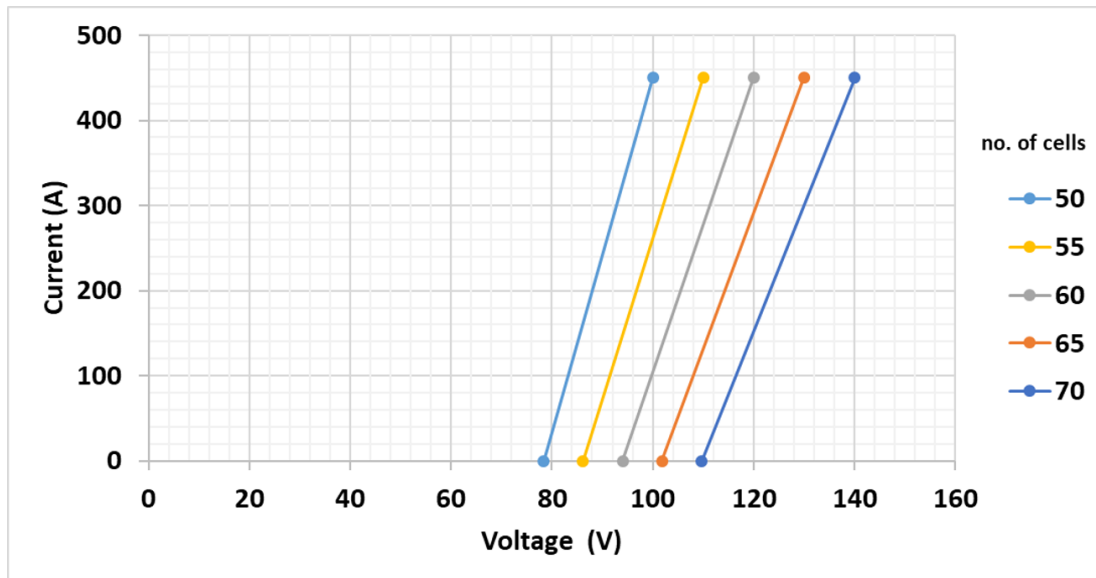


Figure 2.12: Effect of Varying number of cells

Effect of Varying active cell area and number of cells together

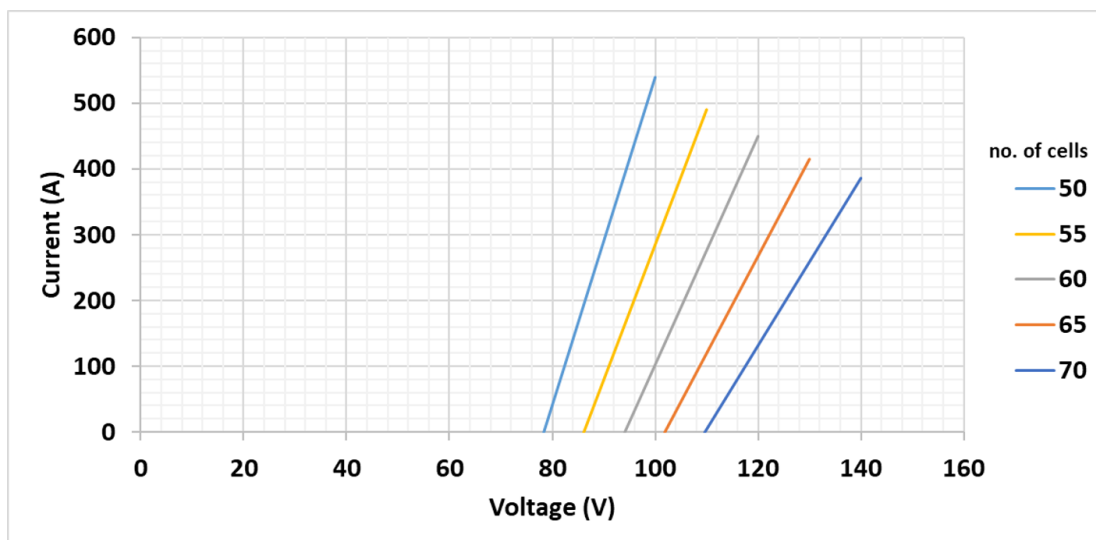


Figure 2.13: Effect of Varying Active Cell area and number of cells together

As it was proved in previous 2 sections that the kW capacity of electrolyzer changes if either number of cells or active area per cell individually is changes. So, now to maintain the kW peak upper limit constant, both active cell area and number of cells in a stack are changed simultaneously. With increase in number of cells subsequently the active area per cell is reduced in the same proportion and also while decreasing the number of cells the ac-

tive area per cell is increased in the same proportion. This also causes the slope of IV curve to decrease towards the right i.e. with increasing cells per stack as shown in figure 2.13. The slope needs to be reduced because lower current is needed for this lower active area per cell design to keep the peak current density and kW power capacity constant. This type of variation would be used in this study while optimizing the right electrolyzer configuration as it was needed to keep the kW capacity of PV and electrolyzer constant and same while optimization.

For smaller cell areas it is clearly visible that higher current is required, so it may add to higher ohmic losses in the cable carrying current from PV to the electrolyzer.. For curtailing the ohmic losses some additional investment would be required to get bigger cables. The heat transfer to the edges of electrolyzer would also change and could cause relatively bigger variations in temperature on the electrode. But all these things needs to be checked separately using CFD techniques and is not in the scope of this study.

3

Photo-voltaic systems

In this chapter, a brief overview of global potential of PV and green hydrogen production is given. Further the IV curve of PV modules and the factors affecting it are explained.

Sun is a paramount source of energy for our planet, which directly or indirectly is the source for most of the renewable energy sources known today. Sun radiates around $6.33 \times 10^7 \text{ W/m}^2$ of energy from its surface and the around 1367 W/m^2 reaches the earth's outer atmosphere. This huge loss happens while the sunlight in electromagnetic wave form travels in the space from the sun towards the earth. As can be seen in figure 3.1, over 50% of land receives over 2000kWh/kWp on earth. Depending on the location of different countries the irradiance varies over the globe, the land between line of Cancer and line of Capricorn receives the highest irradiance. These highest irradiance regions are the regions marked with dark red color in figure 3.1. Depending on the extent of irradiance various regions have varying PV power potential.

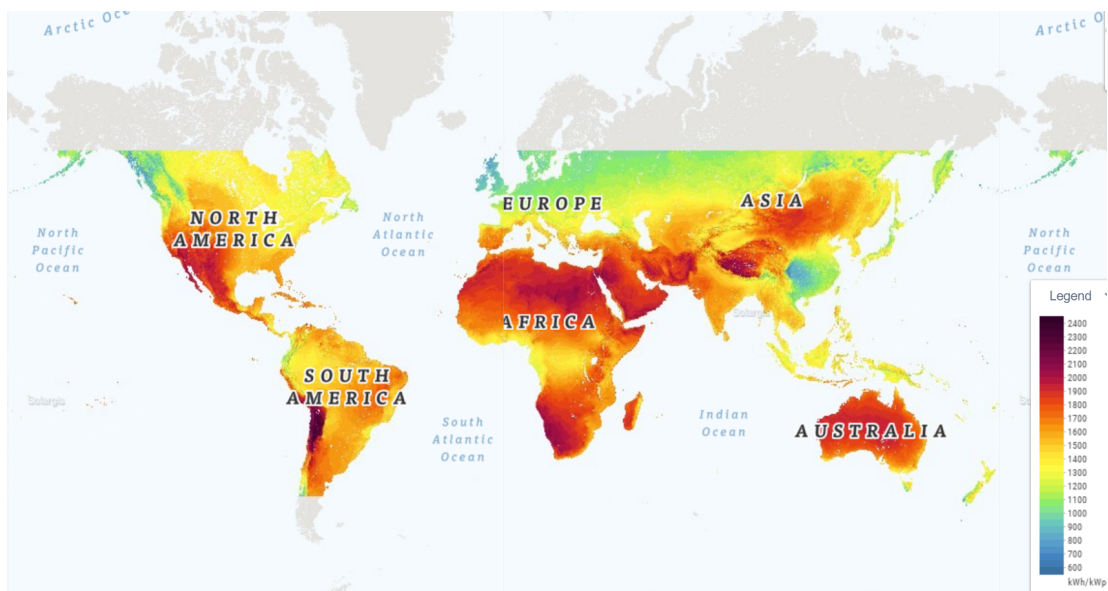


Figure 3.1: Global PV potential SOLARGIS (2020)

Added to variability of irradiance over the globe, the irradiance also varies for one particular

region throughout the day and also seasonally through out the year. Even with high-tech equipment and years of study the weather forecasting is not 100% accurate and always dependable. Renewable energy sources have a high magnitude of intermittency with varying seasons and also during the hours of a single day itself. This intermittency problem needs a storage capacity to balance the supply and demand variations. Hydrogen is seen as a solution for this storage problem, as it can be produced using electrolysis from the power generated by renewables. Hydrogen from solar can be produced only in regions with good irradiance and adequate land availability. At a global scale, countries with higher irradiances can produce this solar fuel (hydrogen) and export it to countries with less irradiance and less land.

3.1. Single diode model

Operating points for a PV module is represented by an IV curve which is a fixed set of points for constant cell temperature and irradiance. For getting this IV curve, a electrical equivalent of solar cell is considered emulating its internal losses like recombination, internal resistance etc. The voltage and current relationship for this electrical equivalent a single diode model is used as shown in equation 3.2. The electrical equivalent circuit is shown in figure 3.2.

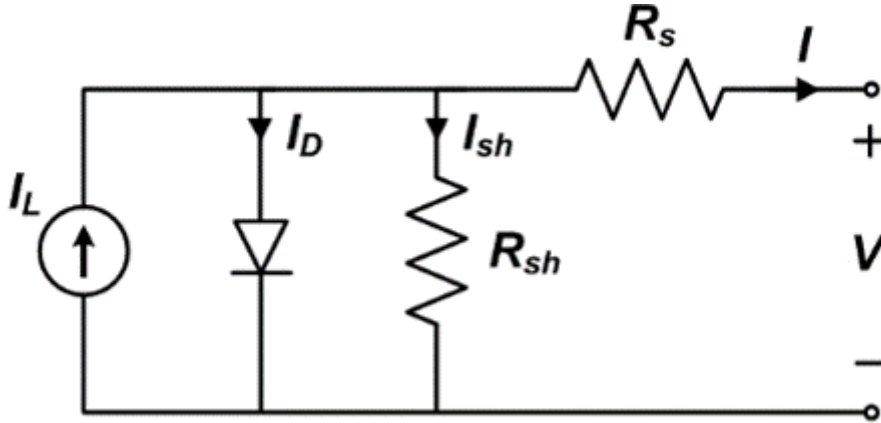


Figure 3.2: One Diode Model- electrical circuit equivalent of solar cell (Sandia National Laboratories, 2018)

The single diode model is given by the following equation,

$$I = I_L - I_d - \frac{V + I * R_s}{R_{sh}} \quad (3.1)$$

$$I = I_L - I_o * \exp\left(\frac{q * (V + I * R_s)}{n * k * T}\right) - \frac{V + I * R_s}{R_{sh}} \quad (3.2)$$

I_L is the photo-generated current in the cell due to impinging irradiance over itself and I_d is the recombination current losses. The series (R_s) and shunt (R_{sh}) resistances of the cell contribute to some additional losses as well. Series resistance is caused by internal resistance to flow of current in cell layers, semiconductor-metal contact interface and the resistance of metal contacts it self. Shunt resistance is mainly due to the internal manufacturing defects

of the cell, which provides an extra route for the current to escape. All these losses and other losses like mismatch losses brings down the PV efficiency below 29% efficiency range. The IV curve generated by a solar cell and also its single diode model is shown in figure 3.3 (Laboratories, 2020).

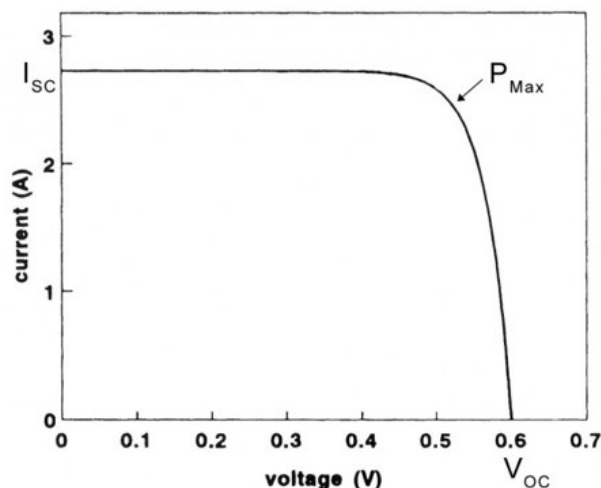


Figure 3.3: IV curve of PV module

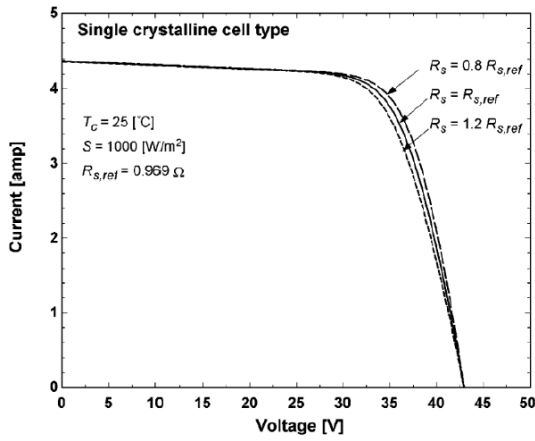
I_{sc} is the short circuit current, it occurs when both terminals of solar cells are short circuited. V_{oc} is the open circuit voltage which occurs during no load condition. P_{mpp} point is the optimum operating point on the IV curve where the solar cell gives the maximum output. Ideality factor denoted by n , R_{sh} , R_s in the single diode equation determines the shape and slope of the IV curve.

Effect of varying R_{sh} , R_s and n on IV curve

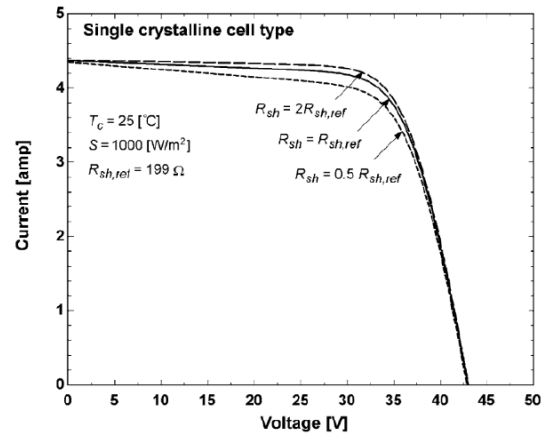
The increasing R_{sh} value causes higher current output for the same voltage, this can be seen in figure 3.4b. The slope of the curve near I_{sc} is $1/R_{sh}$, so the shape of the curve from I_{sc} to I_{mpp} points heavily depends on R_{sh} . Similarly, when R_s is increased, the current decreases for the same voltage. These values may vary for different modules causing varying IV curves amongst them and thus the maximum operating point also changes with it.

3.1.1. Five parameter model

For a PV module, only data like I_{sc} , V_{oc} , V_{mpp} and I_{mpp} would be available on the datasheet. Various methods have been proposed in the literature for finding the other parameters like R_s , R_{sh} and ideality factor (n). One such approach is the five parameter model. In this, the known parameters from the module datasheet are used to form multiple equations from equation 3.2. Then these equations are solved to find R_s , R_{sh} and n . One such method used by SNL's model is by using the Lambert W function (Hansen, 2020).



(a) Variation of IV with varying R_s

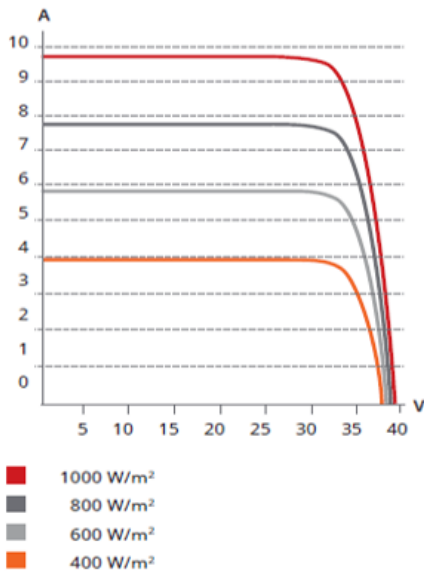


(b) Variation of IV with varying R_{sh}

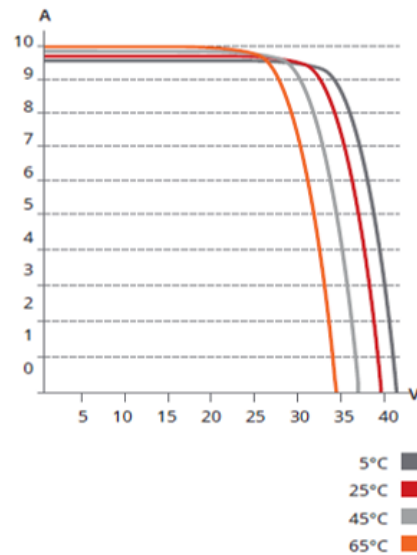
Figure 3.4: Variation of IV with varying R_{sh} , R_s

3.2. Effects of varying irradiance on IV curve

Irradiance on a PV field can vary in time and space causing change in the IV curve and thus the operating points of different PV modules. As shown in the first graph of the figure 3.5a, increasing irradiance causes increase in performance of the PV module. This is clearly due to extra electron-hole pairs formed at higher irradiances. Current produced is directly proportional to irradiance, therefore the current is increasing with irradiance. The voltage increases as well but logarithmically, therefore comparatively the increase is less.



(a) Variation with varying Irradiance



(b) Variation with varying Temperature

Figure 3.5: IV graph varying with Irradiance and Temperature

The irradiance can also vary in space over the PV farm. When modules are connected in series the voltages of each module gets added and the current is matched with the one

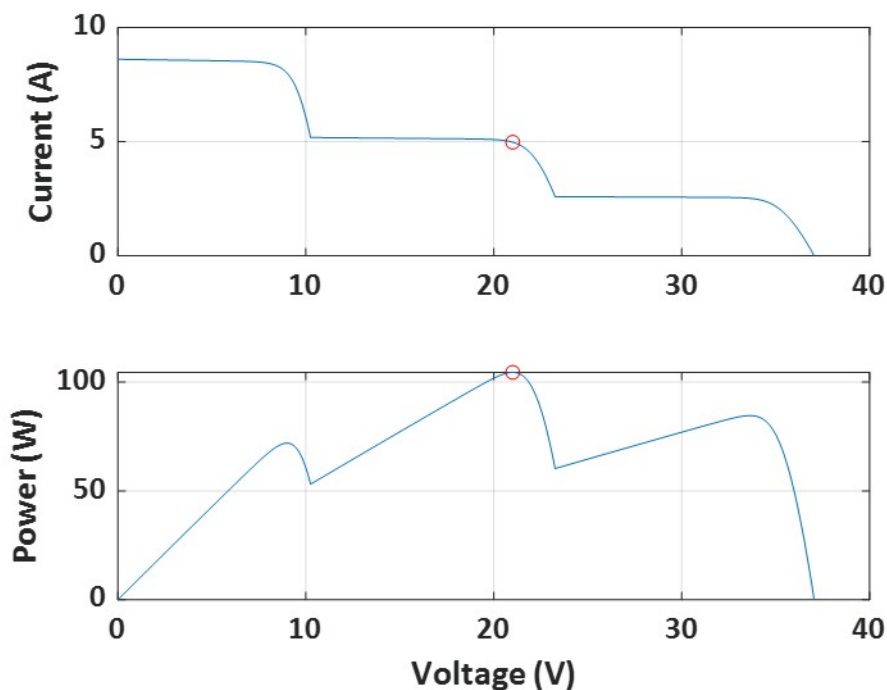


Figure 3.6: Stepped IV curve

producing the lowest current. In-case where the modules are equipped with bypass diodes they form a single stepped IV curve as shown in figure 3.6. The maximum is produced from each modules depending on the irradiance falling on it, the rest extra current in each module flows through its bypass diodes.

3.3. Effects of varying temperature on IV curve

Temperature increase has a deteriorating effect on the voltage of PV module. Increase in temperature increases the recombination inside the PV cells and decreases the bandgap, which leads to decrease in voltage. The current produced increases slightly on the other hand as shown in figure 3.5b.

3.4. Effects of variability of module parameters

The module parameters like I_{sc} , V_{oc} , V_{mpp} and I_{mpp} given on module datasheets are the measurements for that one particular model that was tested for certification. But a variation of 2.5% in I_{sc} , V_{oc} , and 1.5% in mpp points can be expected. The variation could increase even further upon ageing of modules. These changes in individual modules of PV array would cause the individual IV curves to vary even at same ambient conditions. This may resemble like the case where each module gets different irradiance and thus would get a stepped IV curve as shown in figure 3.6.

4

Working of direct coupling PV - Electrolyzer system

In this Chapter, first the working of Direct coupling would be explained in brief. Then in section 4.1, some of the literature pertaining to directly coupled systems would be discussed in detail. The literature would be divided in to two sections based on the system size. The current physical setup installed at STCA and the newly planned weather station would be discussed in section 4.2.

4.0.1. Directly coupled configuration

The most elementary way for producing hydrogen from solar is by directly connecting the solar farm to the electrolyzer, and this configuration is called PV-Electrolyzer direct coupling configuration and is shown in figure 4.1. It is devoid of any power electronics, which reduces the complexity as well as extra costs associated with it. Only controls that is present is at the electrolyzer end for safety reasons. A switch which disconnects the whole system if the incoming current is lower than the safety limit, as was seen earlier in chapter 2 that the hydrogen crossover occurs below this safety limit.

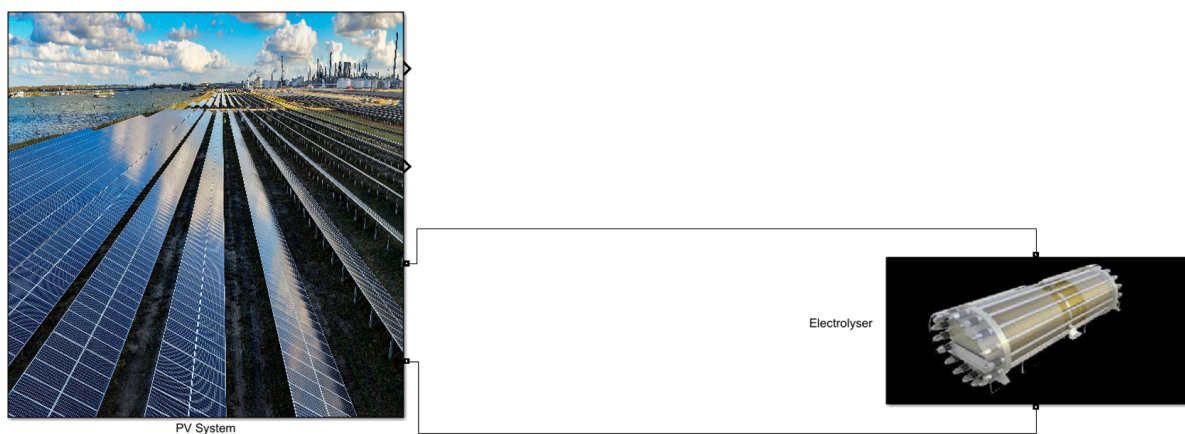


Figure 4.1: Directly Coupled System

The green curves in the figure 4.2 are the IV curves from PV, with each of its MPP point marked in red. The blue line represents IV curve of electrolyzer. The only operating point for

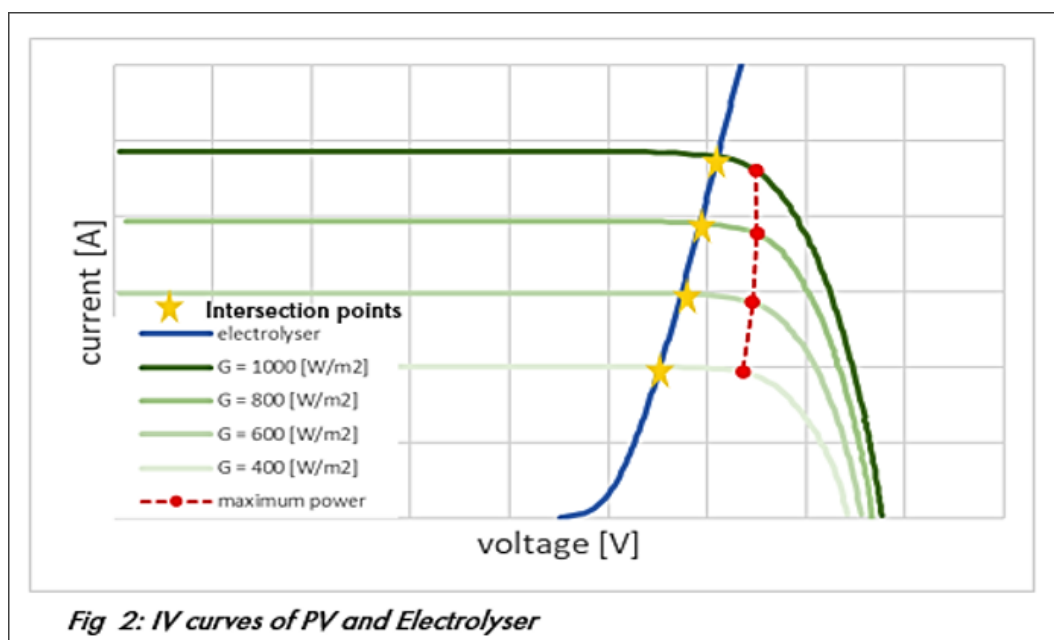


Figure 4.2: Operating Points of Directly Coupled Systems

this configuration is the intersection points of IV curves from both PV and electrolyzer side which is shown in the figure 4.2 with yellow stars. The operating point can't be controlled in this type of coupling, the weather conditions determine the IV curve of PV systems and the temperature determines the IV curve of electrolyzer. It can be seen in figure 4.2 that the operating points are a bit away from the MPP points, that results in under-utilization of available power from solar. For understanding how well the available power is utilized, coupling efficiency is used as an indicator during this whole study. Coupling efficiency is defined by power supplied to the electrolyzer with respect to the sum of maximum available power from each module at a given weather condition. The coupling efficiency is given by :

$$\eta_{coupling} = \frac{\text{Power Supplied to Electrolyzer}}{\text{Sum of MPP power of each PV module}} \quad (4.1)$$

The main aim of this project is optimize this efficiency for the configuration, considering the irradiance variation, module parameter irregularity. This would be done by changing configurations of PV modules in series or parallel along with changing number of cells in electrolyzer stack. There is already many attempts done to understand and optimize this direct coupling systems, which would be reviewed in the next section 4.1.

4.1. Literature review of PV-Electrolyzer systems

Until now, there have been multiple studies on coupling PV and electrolyzer systems. Few of the demonstration projects and researches were already mentioned briefly in the section 1.2. Here in this section 4.1, every type of study done would be divided according to the system size used, time scale of data and the variations accounted in the input data for the model while optimizing the right configuration.

4.1.1. Literature review of direct coupling systems

Studies Using Single PV Module

Starting with the research conducted by Rahim et al. (2015), which was a modelling project using one 60W PV module and an electrolyzer stack where its cells were varied. An attempt to match the MPP points and electrolyzer was done to using their mathematical models. For electrolyzer model he used the model and its constants given by (Ulleberg, 2003) in his paper. He showed that a coupling efficiency of order 99.17% can be achieved by varying the electrolyzer cells in the stack. But it could be observed in his electrolyzer curves that while increasing the electrolyzer cells he kept the active area per cell constant. Thus, with increasing cells the capacity of electrolyzer cells increased in terms of watts but PV remained constant at 60W, so it was clearly a case of over or under designing at the electrolyzer end. The irradiance variation only in time was considered and not in space for PV modules. While doing the optimization just the $1000\text{W}/\text{m}^2$ IV curve of PV and IV curve of electrolyzer at 80°C was used and the rest were ignored, thus it is required to see if a single electrolyzer curve can give this kind of efficiency above 99% for all IV curves of PV at each irradiance.

García-Valverde et al. (2011) tried optimizing the direct coupling configuration of PV-Electrolyzer setup too but in a slightly different way. He collected weather data for two years for a particular orientation of PV module and then a cloud of MPP points were plotted on I vs V graph as shown in figure 4.3, all the points on this graph are normalized with MPP points at STC. Two PEM electrolyzer were modelled using data from Takasago plant and UPCT plant. The electrolyzer curves are optimized in this region of MPP points from the PV module. All the temperature varying IV curves for both electrolyzer were optimized. The MPP point region for single module and for multiple modules in series would change in shape, which should be accounted for but here it is not considered.

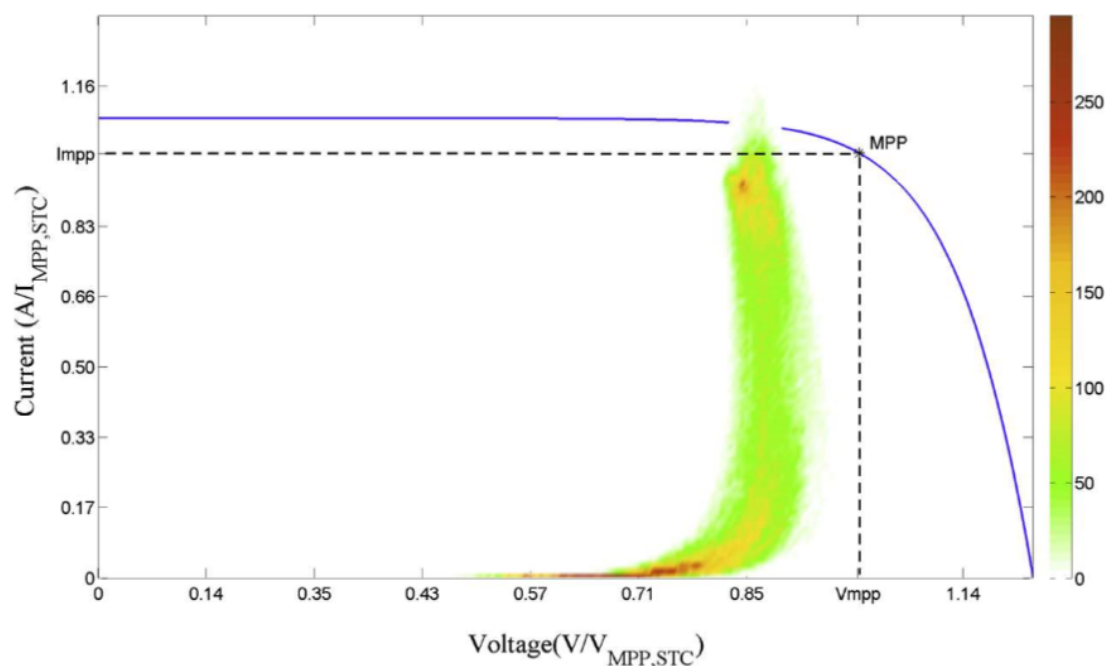


Figure 4.3: MPP region for 2 years, (García-Valverde et al., 2011)

A more sophisticated optimization for correct PV-electrolyzer configuration was done by Maroufmashat et al. (2014). In this research, Imperialist Competitive Algorithm approach was used to find optimized results. A multi-objective non linear optimization was performed. First objective was to maximize the energy transfer from solar to electrolyzer and second was to maximize the hydrogen production. Number of PV panels in series/parallel and number of electrolyzer cells was optimized like other configuration optimizations but here an additional variable of water activity was considered too for evaluating optimum conditions for reaction. Water activity is the partial vapour pressure of water with respect to water saturation pressure (Maroufmashat et al., 2014). He observed that the optimum for minimum energy loss and maximum hydrogen output were conflicting, for which he suggested the use of Pareto curves to trade off between variable. (Laoun et al., 2016) did a similar work where he optimized the directly coupled PV-electrolyzer systems using his own model, which was a tool that could be used for any geographic location. The electrolyzer side of the system was over designed with respect to one PV modules attached to it.

Instead of changing the configuration of PV or electrolyzer, the optimization can be done by changing the concentration of hydroxyl ions in the electrolyte was shown in the study by de Fátima Palhares et al. (2018). But in this study, other parameters were not changed and the electrolyzer was undersized, hence a very high efficiency was not achieved. Djafour et al. (2011) modelled 2 PV module system connected to 50W electrolyzer manufactured by them. It was observed that the existing practical model gave a high coupling loss, which stayed below 60% for most of the time. Therefore, they proposed to simulate and find the most optimal configuration for this coupling, for which the electrolyzer cell configurations were changed in the simulations. The new found configuration showed the possibility to run this system above 90% coupling efficiency.

Studies using kW scale PV module

Clarke et al. (2009) did an optimization for directly coupled PV-Electrolyzer system consisting of zero additional components in it. They considered PV system of 2.4kW and starting with a 15 cell, 3kW PEM electrolyzer in which the number of cells could be varied in stack. One thing to be noted is that the number of cells in electrolyzer was increased or decreased while optimizing but keeping the cell active area size constant. This causes oversizing or undersizing of electrolyzer in terms in kW. The PV system was modelled by approximating the single diode equation where the series and shunt resistances and for the electrolyzer the actual measured data from the one manufactured by them was used. With modelling they could achieve a configuration with more than 99% coupling efficiency, in which 15 parallel arrays with 2 PV modules in a string was connected to 16 cells stacked electrolyzer. They complimented this modelling work with a 4 month long experimental study as well. But due to unavailability of 16 cells stack of electrolyzer, a 13 cell stack electrolyzer was used. The experiments showed safe working of direct coupling systems but comparatively a lower coupling efficiency of 88%.

Maeda et al. (2016) showed that it was practically possible to optimize directly coupled system by continuously varying capacity at electrolyzer end. A 2.6kW PV array was connected to 15 cell electrolyzer with an option to control its operable cells as shown in figure 4.4. Three double cells and a single cell were connected with a switch, they were turned with respect to the available power at the PV system end. This control ensured that the elec-

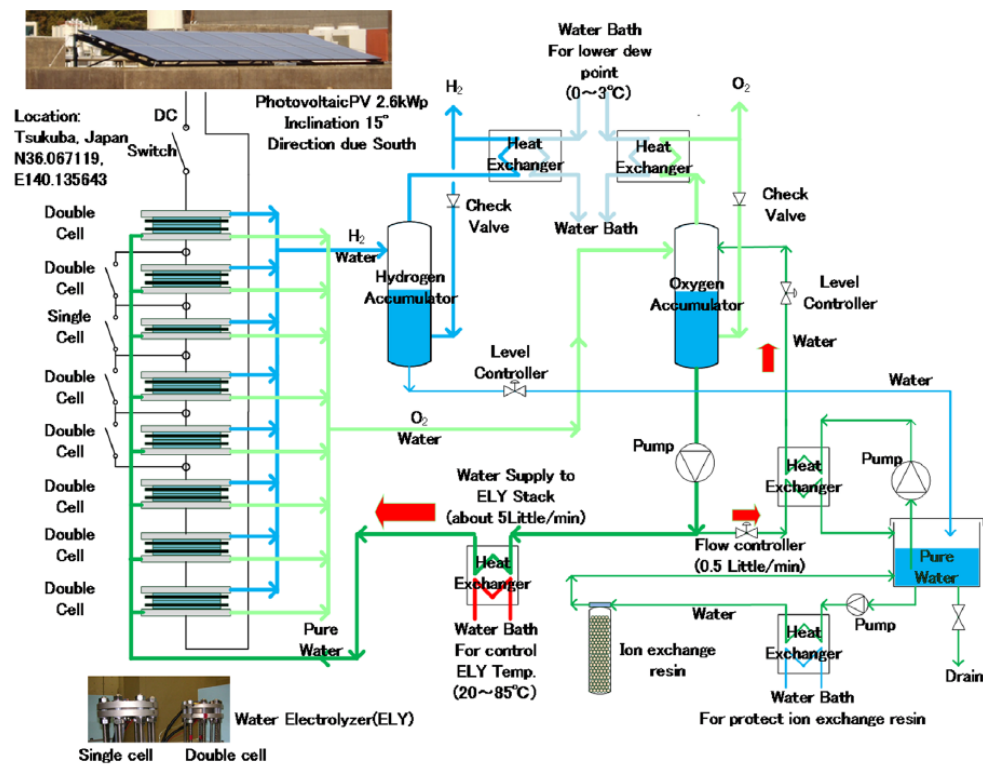


Figure 4.4: Maeda et al. (2016) Setup

trollyzer IV curves were always at the closest possible position with respect to MPP points of PV. The IV curves of electrolyzer were obtained from the available setup. Coupling efficiency of 96-98% was observed during the course of experimentation.

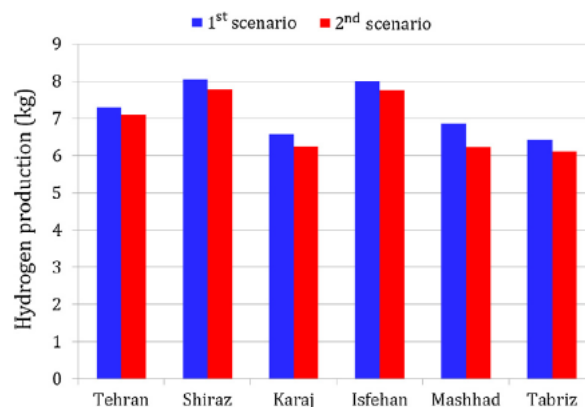


Figure 4.5: H₂ production in the 6 cities (Sayedini et al., 2016)

Sayedini et al. (2016) optimized the PV-Electrolyzer systems for two different scenarios, firstly where energy transfer loss was to be minimized and secondly where levelized cost of hydrogen was to be minimized. Optimization was performed for 6 different cities in Iran, for which hourly irradiance per year was considered. For both the scenarios the optimum

values of PV modules in series/parallel and number of electrolyzer cells in stacks were different. The coupling efficiency for all cities in both scenarios were above 90%, but there was a small decrease in efficiency when the second scenario i.e optimizing of leveled cost of hydrogen was considered. As the second scenario concentrates more on decreasing the hydrogen production cost and not the efficiency and thus also produces less hydrogen as shown in figure 4.5.

4.1.2. PV-Electrolyzer systems with additional components

There were other studies for PV-Electrolyzer systems where additional components were used to stabilize the system, which would be explained in this section. Many of them used batteries to stabilize the power reaching the electrolyzer from varying renewable energy sources or a complete hydrogen production and consumption system was modelled with fuel cells. One of such earliest study was performed in the period of 1986-1997 in Neunburg, Germany. Here, two PV farms of $135kW_p$ and $131kW_p$ were installed as the varying power sources but connected to the DC bus bar via dc-dc converters. The system here used the grid for stabilizing the system. A low pressure $111kW_p$ alkaline electrolyzer, $100kW_p$ high pressure electrolyzer and a $100kW_p$ PEM electrolyzer were tested for hydrogen production. This test facility also comprised of testing facility for the final use of hydrogen too, therefore two fuel cell plants of total $85kW_p$, $10kW_p$ fuel cell forklift, $66kW$ of various heating systems using natural gas in combination with hydrogen and a refrigerator with catalytic burner was tested. Though the span of project was almost half a decade but the operating hours were relatively modest except for low pressure alkaline electrolyzer which ran for almost 5000 hours. There were breakdowns and glitches in many parts of this test facility due to the use of many prototype elements but for later 7 years it could run safely. Many researches like Aki et al. (2018) have used grid to stabilize the system.

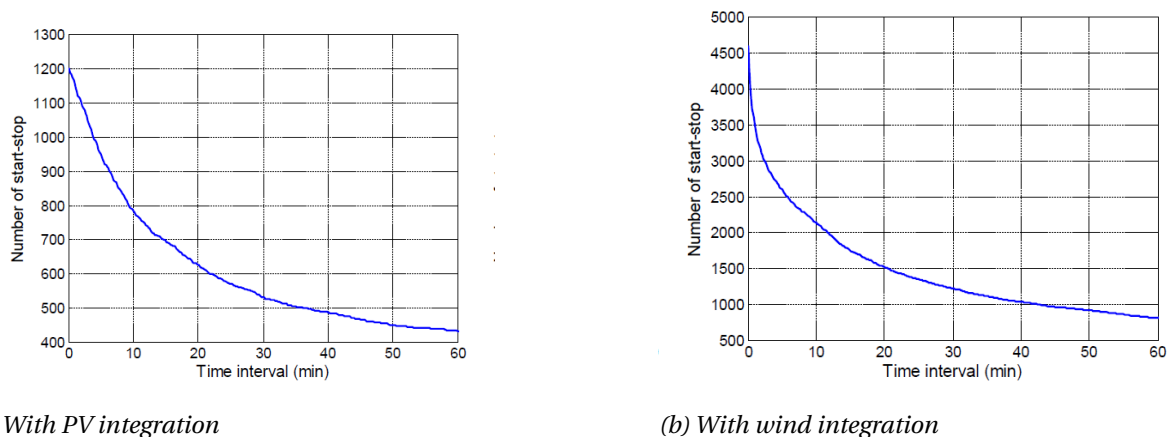


Figure 4.6: Number of start-stops for electrolyzer with PV integration and wind integration, (Ursúa et al., 2016)

Ursúa et al. (2016) used $6.8kW_p$ of solar and $6kW$ of wind together as a varying renewable generator connected to an alkaline electrolyzer via power converters, to evaluate the main limitations of this configurations. The main limitations that could be seen from the results was that the number of start-stops were quite high and thus resulting in high loss of power

generated. To limit the start-stops he proposed two solutions, one was to increase the interval of time for which the operation of system is continued even after breaching the lower safety limit. As can be seen in figure 4.6a and 4.6b, as this interval for completely stopping the electrolyzer post breaching of lower limit is increased, the number of shutdowns decrease gradually for both PV and wind integration. It was found that electrolyzer can keep itself operational for 10 minutes interval safely without forming an inflammable mixture of hydrogen and oxygen. This limit is different for each electrolyzer vendor. The second option where the stops reduced even further was by the use of batteries but it was without any consideration of cost impacts. With the use of batteries, the stops are almost halved in numbers.

From the literature it is clear that many of the optimizations and feasibility studies were done for single module setups. Even the kW scale projects didn't take into account the variations in IV curve that maybe caused due to irradiance variation across the field or variation in module characteristics. While optimizing for the best configuration of PV-Electrolyzer, the cells in electrolyzer stacks were increased or decreased without changing the active cell area which would cause increase or decrease in kW capacity of electrolyzer. In the current study, the active cell area is changed accordingly with number of cells in electrolyzer stack to keep the kW capacity of the system same. Variations in PV module characteristics and irradiance variations in space over the modules do affect the PV-electrolyzer systems performance and they are included and studied in this project. Additionally, the ohmic losses were ignored by most of the studies as well, which would be included in the current one and the significance of its inclusion would be explained using the results.

4.2. System configuration and simulation results of the STCA setup

In this section, the current weather station and the new weather station to be installed would be discussed. The missing data taken from databases or calculated using models would be explained. The current setup of modules and electrolyzer setup at STCA, Amsterdam would be explained and results from the same would be explained.

4.2.1. Understanding the irradiance and module temperature to be measured

The extra-terrestrial irradiance that reaches the boundary of earth's atmosphere is 1361 W/m². This irradiance gets refracted and dispersed in the earth's atmosphere before reaching the earth's surface. The irradiance that reaches the ground is the Global Horizontal Irradiance (GHI), which is the combination of different components, namely, Direct Normal Irradiance (DNI)/ Beam Irradiance and Diffused Horizontal Irradiance. DNI is the irradiance which comes directly from the sun without reflection and DHI is the component of irradiance which reaches the surface after at least one reflection in the atmosphere. These irradiance components are shown in the figure 4.7.

It is also important to briefly understand the angles describing the position of sun and PV module, which are shown in figure 4.8 and are defined as follows:

- Solar altitude angle: The angle that direct solar rays from sun reaching the ground makes with its own horizontal projection on the ground is the solar altitude angle and is denoted by α_s in the figure 4.8.
- Solar azimuth angle: The angle that direct solar ray's horizontal projection on the ground makes with the south direction and is denoted by γ_s .

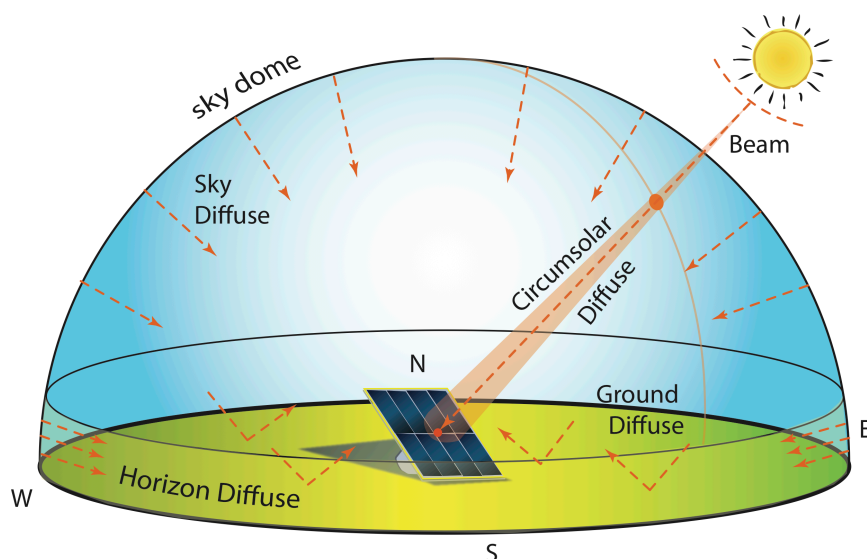


Figure 4.7: Components of Global Horizontal Irradiance, (Jeffrey R. S. Brownson, 2020)

- Module azimuth angle: It is given by the angle made by the horizontal projection of surface normal of the PV module with the south direction and is denote by γ_m
- Module altitude angle: The angle that surface normal of PV module makes with its own horizontal projection on ground.
- Angle of Incidence (AOI): AOI is the angle between the surface normal of PV module and the direct normal ray from the sun and this is shown in figure 4.8 by θ .

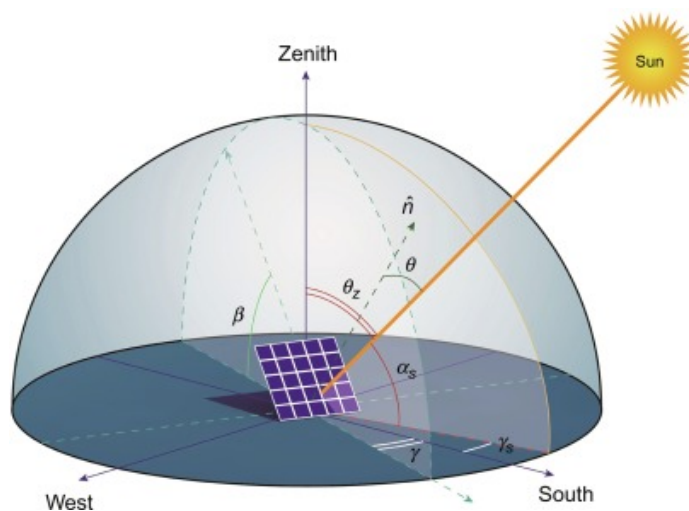


Figure 4.8: Different solar angles, (Rosa-Clot and Tina, 2017)

In the current existing setup the only equipment available on weather station is one pyranometer, which measures the global horizontal irradiance (GHI). For calculating the IV curve using 5 parameter module, the input required are plane of array irradiance and the module temperature. Plane of Array (POA) Irradiance is nothing but summation of all

irradiance components like DHI, DNI and ground reflected irradiance resolved on the plane parallel to surface of the PV module. Some models and additional data from databases were needed in this case as neither the pyranometer was aligned on the plane of array nor a temperature sensor was placed under any module.

Finding the plane of array irradiance

For calculating the Plane of Array (POA) irradiance, you need to know the following:

- Bifurcation of GHI into Diffused Horizontal Irradiance (DHI) and Direct Normal Irradiance (DNI)
- Tilt of Module
- Azimuth and Altitude angles of sun
- Albedo

The total POA irradiance over a module is given by the following equation:

$$POA_{Irr} = POA_{DNI} + POA_{DHI} + POA_{ground-reflected} \quad (4.2)$$

Each component of irradiance like DHI, DNI and ground reflected irradiance is resolved along the POA plane and summed up to give total POA. For now, the ground reflected irradiance as the ground surface for STCA's PV plant is dark grey, whose albedo would be as small as 0.2 or lower was neglected. It would be of greater significance there are white structures near it or if the ground is painted white or if bifacial PV modules are used. DHI and DNI can be obtained by two ways, first by using data from nearby station of Koninklijke Nederlands Meteorologisch Instituut (KNMI) or Meteonorm, who have local weather monitoring stations in Netherlands and can provide hourly irradiance, solar azimuth and solar altitude angle data for Amsterdam. Second way is by using decomposition method to obtain DHI and DNI from GHI and then using transposition models for POA irradiance. Various decomposition models are available to calculate DHI and DNI from GHI. Over past decades many models like Erbs, Perez, Orgill and Hollands, BRL etc have been developed and used for decomposition. Calculating diffuse fraction denoted by k_d is the final aim of the decomposition models. This k_d is given by:

$$k_d = \frac{DHI}{GHI} \quad (4.3)$$

Each of the available models take into account different variables depending upon the sensitivity analysis or previous results. Different variables like k_t (clearness index) which defines the received GHI irradiance with respect to available extra-terrestrial irradiance, solar altitude angle (α), solar azimuth angle (θ_z , ambient temperature, relative humidity, apparent solar time (AST), daily clearness index (K_t) and persistence (ψ) are used in different models. Mostly the models were developed in northern hemisphere with the data for USA or Europe, therefore BRL model was made to decompose GHI for both the hemispheres with similar accuracy (Ridley et al., 2010). The BRL decomposition model is given by :

$$k_d = \frac{1}{1 + e^{-5.38 + 6.63k_t + 0.0006AST - 0.007\alpha + 1.75K_t + 1.31\psi}} \quad (4.4)$$

Once the DHI and DNI components are decomposed from the GHI, further each component of POA is given by :

$$POA_{DNI} = DNI * \cos(AOI) \quad (4.5)$$

$$POA_{DHI} = DHI \times \left[A_i \cos(AOI) + (1 - A_i) \frac{1 + \cos(\theta_T)}{2} \left(1 + \sqrt{\frac{DNI \times \cos(\theta_Z)}{GHI}} \sin^3 \left(\frac{\theta_T}{2} \right) \right) \right] \quad (4.6)$$

Where A_i is anisotropy index which is the ratio of DNI with respect to extraterrestrial radiation and θ_T is tilt angle of the module. Once both the components of POA are found, the global POA can be calculated by their sum.

Calculating the module temperature

A very simplistic model from PVEDUCATION (2019) for calculating the modules temperature was used for this study, which is given by,

$$T_{cell} = T_{ambient} + POA(W/m^2) * \frac{NOCT - 20}{800} \quad (4.7)$$

Where NOCT is the nominal operating cell temperature, which typically lies between 33-58°C. Better models like with accuracy can be used, but they require additional data like windspeed. Windspeed can again be taken from a local ground based weather station and logarithmically can be upscaled to the required height. One such model has been given by Sandia National Laboratory:

$$T_m = E_{POA} \cdot (e^{a+b \cdot WS}) + T_a \quad (4.8)$$

Where a and b are coefficients which depends on the module type and the mounting type.

4.2.2. Weather station installation at STCA, Amsterdam

The figure 4.9 shows the layout and placement of new measurement equipment to be installed at STCA, Amsterdam. The exact location and reason for its placement would be discussed further in this subsection.

In the previous sections it was seen that multiple models were required to final get the inputs needed for single diode model for getting the IV curve. Though these models have been proven to be quite accurate, but all models come together to contribute to some reduction in accuracy. Therefore it is necessary to eliminate these models for better accuracy in calculating the PV output. Additional components are required for studying the varying weather condition effects on the system. The following were mainly required :

- A pyranometer to be installed along the plane of PV modules, which would eventually give the POA irradiance.
- Temperature sensor for the PV module is required for getting exact module temperature.
- Pyranometer for DHI irradiance and Sunshine meter for DNI, to study the effect of diffused and direct irradiance variation on this system.
- Anemometer for measurement of windspeed, for validating the temperature measurement from module using equation 4.8.
- A sky scanner to monitor the cloud coverage and its movement.

Two pyranometers were installed for POA irradiance measurement, one on west facing and another on east facing PV module. It needs to be free from obstructions at 5° above horizon. The pyranometers are placed adjacent to PV panel number 82 for west facing modules and

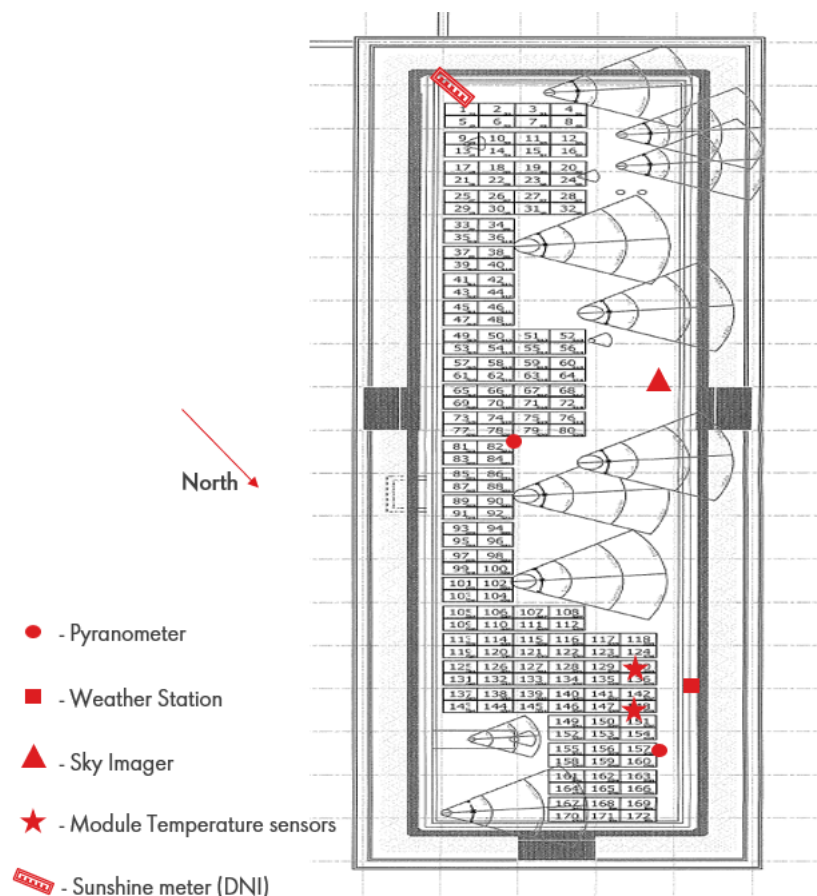


Figure 4.9: Equipment Placement

PV panel number 160 for east facing modules. The nearby chimneys were bright metallic colour, therefore it is covered with black matte finished sheet as seen in figure 4.13 to avoid reflection from it.



Figure 4.10: Sunshinemeter from EKO Instruments

A sunshine meter was placed on the south west corner of the roof. This sunshine meter was used for measuring the DNI. It is quite different than the usual pyrheliometer which rotates and track the sun constantly for the direct irradiance as shown in figure 4.10.

In this device from EKO instruments, there is a small reflecting mirror inside the glass tube which rotates 360° for about 15 secs or more as per the settings by user. As shown in figure

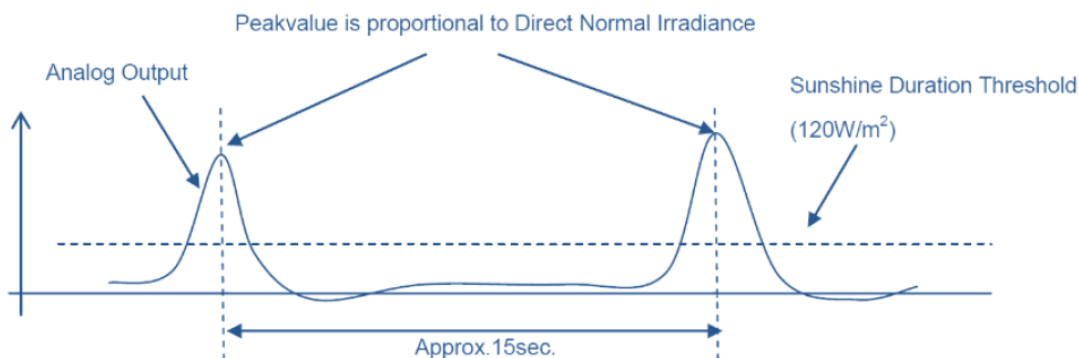
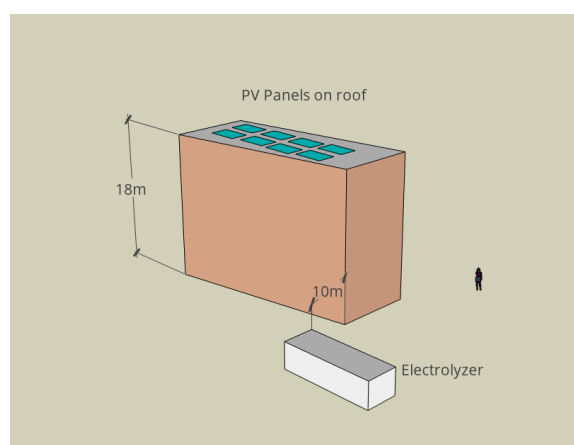


Figure 4.11: DNI peaks in 15 secs, ((Pó et al., 2018))

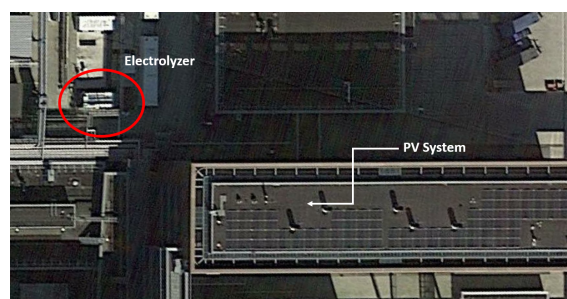
4.11, during these 15 secs it searches for the peak irradiance in all direction and when it is directly facing towards the sun with AOI zero, it records that analog signal as the DNI (Pó et al., 2018). It needs to be facing south for installation in northern hemisphere.

A weather station was placed to which a anemometer is connected to get the windspeed data. It also has temperature measurement equipment for ambient and module temperature. This weather station was to be installed at least 30m away from any obstruction which is taller than 2m. But the furthest, the weather station could be kept from chimneys was 15m at the specified location in figure 4.9. A sky imager was placed 1.5m adjacent to module 64. This device gives high resolution images and data analysis report of the cloud movement and sun's location.

4.2.3. Current setup of PV modules and Electrolyzer stack



(a) Sketch of PV- Electrolyzer setup at STCA



(b) Google Image

Figure 4.12: PV-Electrolyzer set-up at STCA, Amsterdam

A 50kW PV-Electrolyzer system has already been setup at STCA, Amsterdam campus. As shown in the figure 4.12a, The PV panels are installed on the roof top of a building in the campus which is almost 18m in height and the electrolyzer is placed on the ground level

adjacent to this building which are diagonally 10m way.



Figure 4.13: STCA Rooftop Installation

A 51.24 kWp PV system is installed on the building roof. It consists of 168 modules from Canadian Solar CS6K-300MS connected in east-west configuration as shown in figure 4.13. 4 panels were connected in series and 48 such arrays were connected in parallel. An alkaline electrolyzer of 50kW was directly connected to this PV system. This electrolyzer turns on only when the irradiance is above $350\text{W}/\text{m}^2$. If the irradiance falls below this irradiance for prolonged time then it switches off to avoid hydrogen crossovers. At lower current densities during low irradiance period, the oxygen production goes down rapidly and there is big pressure difference between oxygen and hydrogen side. This may cause the hydrogen to go on the other side and form a explosive mixture with oxygen.

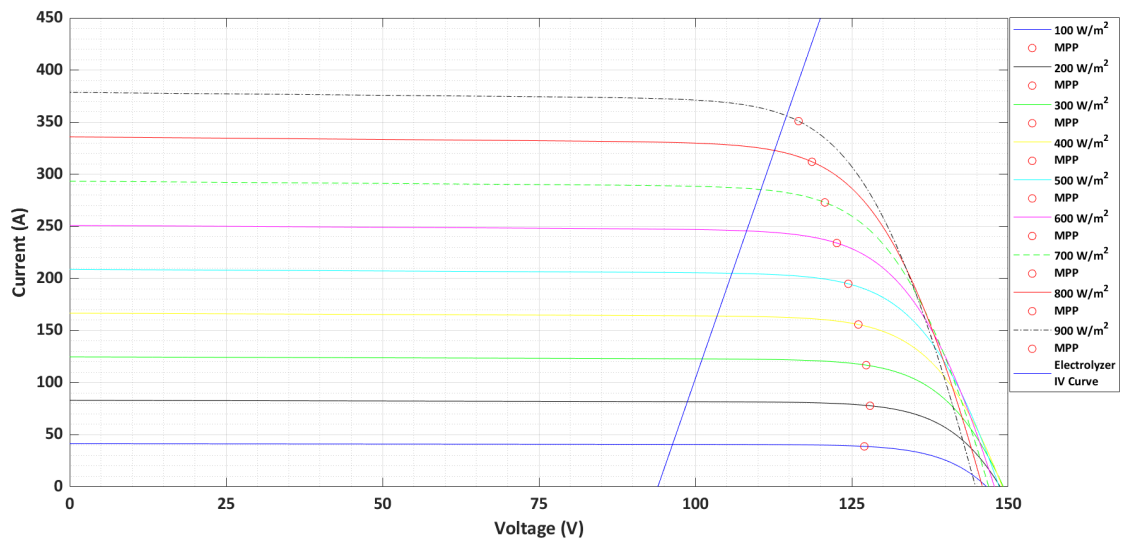


Figure 4.14: IV curves of PV and Electrolyzer

In this directly coupled system, the irradiance and module temperature decides the available set of operating points i.e the IV curve of PV. Then the single final operating point for those conditions is decided by intersection of IV curves of PV and electrolyzer. The simulated IV curves from PV and electrolyzer for setup at STCA is shown in figure 4.14. The IV curve of PV system is given in different colour and is increasing in amplitude with increasing irradiance, these various irradiance values are seen through out the day varying with time.

The MPP points of PV are marked in red circles and the single blue colour straight line is the electrolyzer IV curve. The operating points are the intersection points of these curves. The coupling efficiency is decided by the distance between this operating point and the MPP point of the PV. It can be seen that the efficiency decreases with decreasing irradiance due to the slope of electrolyzer IV curve.

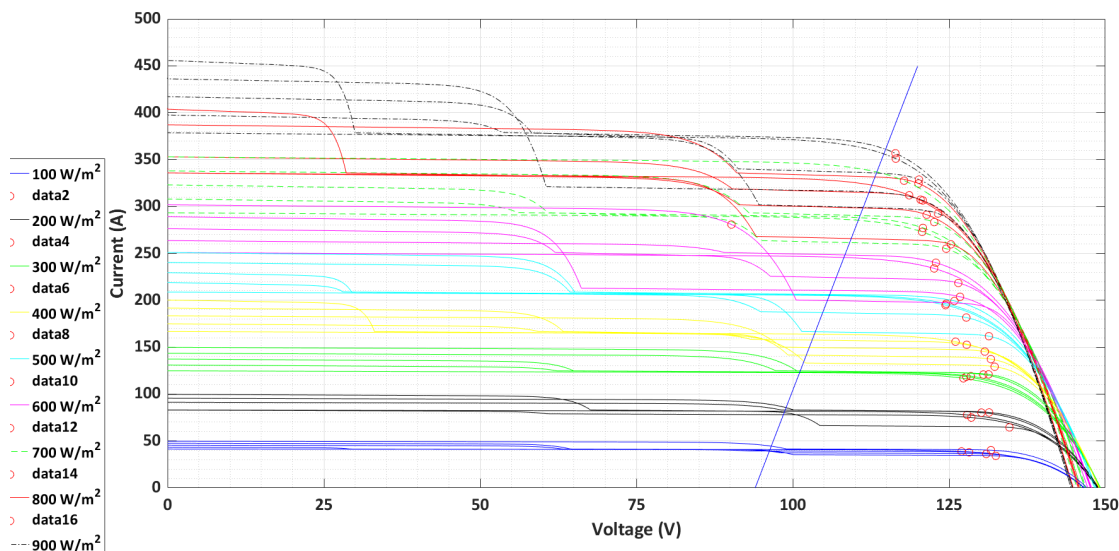


Figure 4.15: Variation in Irradiance and module parameters

In this case for the available electrolyzer this configuration of PV i.e. 42 strings in parallel and 4 in series was the best possible configuration to have electrolyzer IV curve and solar MPP points as close as possible. In this case all the modules were considered identical and also the irradiance was considered uniform in space, therefore all the 168 modules had same IV curve. Hence the final IV curve was obtained by adding up the voltages in series and current in parallel to get a smooth IV curve. But in real life situation the conditions could be quite different, there could be a space variation of irradiance falling on each of the modules or degradation of modules or no uniformity in modules. These situations will cause changes in the individual IV curves coming from these modules. In figure 4.15, the steps in IV curves of PV at each irradiance can be seen. These steps were due to variation in irradiance or variability in module characteristics.

During a webinar by Eternalsun spire, a leading solar simulator company showed that there was a deviation of $\pm 5\%$ deviation observed amongst same brand of modules (Pepijn, 2020). A comparative characterisation of PV modules was done simultaneously in many labs across Europe by Stellbogen et al. (2010). In this test, institutes from Estonia, France, Germany, Great Britain, Poland, Spain and Switzerland simultaneously recorded the IV curves in ambient conditions and then translated the data to Standard Test Conditions of $1000\text{W}/\text{m}^2$ and 25°C for comparison. It was seen that the modules showed upto 5% deviation in short circuit current and upto 2.5% deviation in maximum power point. These variations are observed even before the installation of modules. Now once the module is installed, environmental factors do impact the performance variably as well. It is seen that due to soiling upto 2% of losses can be induced to the total losses occurring at individual module (Nepal, 2018). This soiling loss could be non uniform on the modules based on the

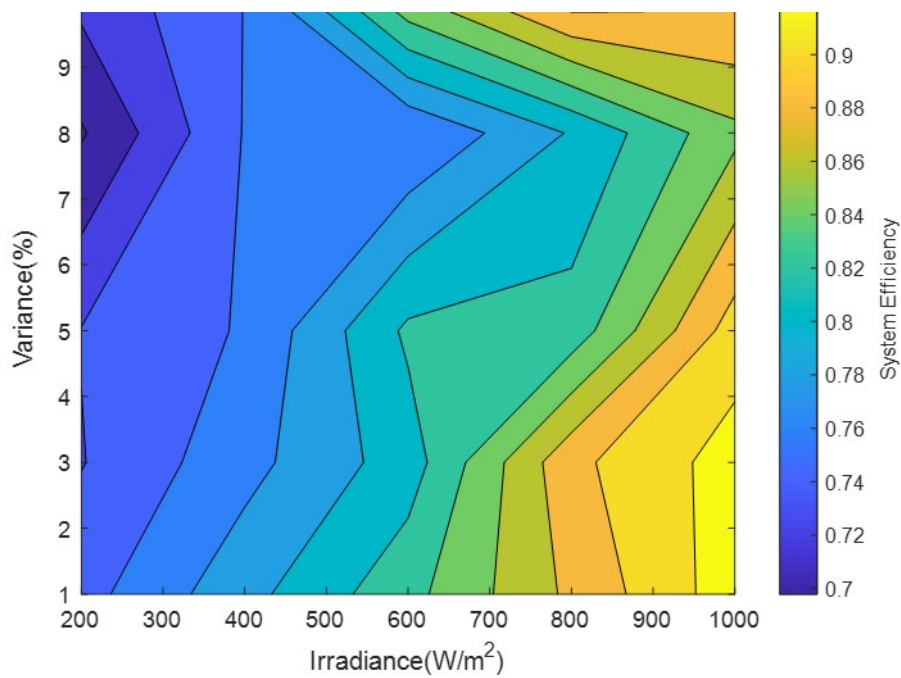


Figure 4.16: Heatmap of Coupling Efficiency with variation in Irradiance

wind direction and its orientation. Bird droppings could lead to similar losses as well. Post the use of modules, it undergoes degradation over its lifetime and the external parameters of individual modules do change. In study a conducted by Saadsaoud et al. (2017), where PV modules were tested after a use of 12 years on fields in Algeria. It showed that there was a yearly 2% decrease in rated of the module, 2.75% decrease per year in I_{sc} . With this rate the modules will degrade almost 20% in 10 years, therefore understanding of these situations is also needed.

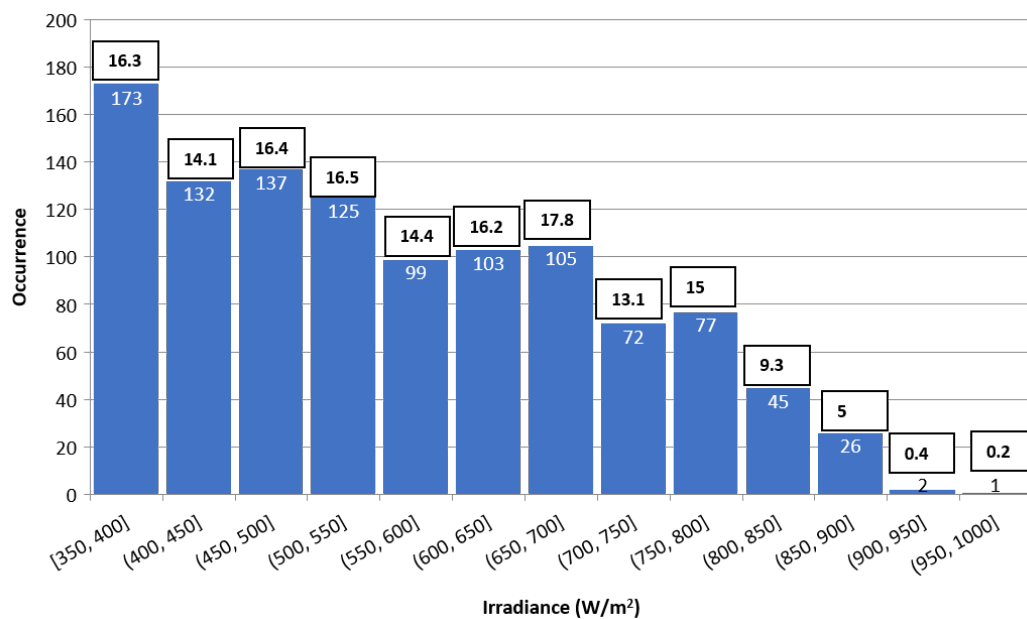


Figure 4.17: Histogram of yearly irradiance and energy produced in MWh

A variation of 0 to 20% was applied across the modules in string and in parallel arrays. The magnitude of the variation did affect the IV curves differently and thus the coupling efficiency too. It can be seen in the figure 4.16, that the coupling efficiency increases with irradiance. This was expected as can be seen from 4.15 the MPP points at higher irradiance were closer to electrolyzer curve compared to MPP points at lower irradiance. With increased variance in irradiance or the module parameters, the coupling efficiency dropped too. The drop was significant, which dropped till 70%. As can be seen in figure 4.16, the coupling efficiency for the irradiance range of $200-600\text{W}/\text{m}^2$ was as low as 70-80% which is quiet low compared to the achieved 95% and above as found in the literature. Additionally, the alkaline electrolyzer losses around 30% of its energy in the form of heat while converting electricity to hydrogen. Therefore, efficiency above 90% should be achieved for all variations in irradiance or module parameters.

As can be seen in figure 4.17, the irradiance range of $350-700\text{W}/\text{m}^2$ contributes to maximum energy production. The white text boxes over the histograms give MWh energy production per year from the irradiance falling in that particular range for this 50kW PV system set-up at STCA. The occurrences are highlighted inside the histograms in white. The occurrences of the irradiance values in the range $200-600\text{W}/\text{m}^2$ is the highest in a year. Therefore, optimization of coupling efficiency for irradiance values of this range must be done. In the following chapter a tool for optimizing the direct coupled PV electrolyzer system will be discussed.

5

Understanding the tool developed

This chapter presents the simulation tool for optimizing the directly coupled PV electrolyzer system. The constraints or the boundary conditions that were set for the simulation will be discussed. The importance of considering the ohmic losses and its effects on the directly coupled system will be put forth. Finally, the results from the simulations will be presented and analysed in detail.

5.1. Self-programmed tool

For optimization of maximum energy extraction from PV a tool was developed. The tool was built using MATLAB-Simulink, which is an integration of textual and graphical programming (MathWorks, 2020). The Simulink model is for simulating the IV curves of PV array which is called from the MATLAB script itself. The rest optimization is done using the MATLAB script itself

The tool requires four input parameters, viz., weather data, PV module parameters, number of electrolyzer cells and the active area of these cells. The weather file includes Plane-Of-Array (POA) irradiance on each module orientation (east or west facing). PV module parameters includes number of cells in series in a module, open-circuit voltage V_{oc} , short-circuit current I_{sc} , voltage at maximum power point V_{mpp} and current at maximum power point I_{mpp} .

After providing the input parameters, the size of the PV electrolyzer system is fixed and entered into the tool. To begin with, the first system size selected is for a 50kW system and the optimization was done for the same. After which the tool calculates all possible configurations for the given PV module and the electrolyzer cell stack.

5.1.1. Constraints for the simulation

The possible configurations were filtered out after applying the set boundary conditions, which are explained below,

- Maximum voltage: Presently, the maximum operational voltage limit for any commercially available electrolyzer has been set at 500V. Experts in the field of alkaline electrolyzer agree to this limit. But no literature is available on this hard set limit.

It could be speculated that the electrolyzers above this range are too large that it may have been causing non-uniform degradation of electrolyzer cells in the stack (van Kruijsdijk, 2020). Because of the maximum limit of 500V, the maximum electrolyzer cells allowed in a stack will be 250 considering 2V as the upper limit per electrolyzer cell. Considering the 305W module from Canadian solar, whose V_{oc} is 40V, the maximum PV modules that can be connected in a string should be 12 to be within the 500V range.

- Minimum irradiance: A minimum limit of $350W/m^2$ was set for the irradiance to start the electrolyzer. The irradiance below this limit will cause higher cross-over of Hydrogen to the Oxygen side. This is majorly due to the fact that contamination of hydrogen increases with decreasing current density (Schröder et al., 2004), which approaches the explosion limit. The electrolyzer starts once the $350W/m^2$ irradiance level is reached. But, if the irradiance level drops below $350W/m^2$ during operation post the start, it can maintain the operation for about 10 minutes. For simplicity of simulation only the irradiance above $350W/m^2$ was considered.
- Minimum number of series connected modules in a string: Considering the safety factors that needs to be satisfied for electrical cabling of PV module, A factor of 1.5 is multiplied by to I_{sc} while selecting the cable size. Therefore, single module in a string and rest 168 modules in parallel for the case of 50kW system was rejected as the cabling selection was to be done for 2520A. Such high current would result in high cabling cost if the ohmic losses is to be reduced.

5.1.2. Logic for optimization

The POA irradiance input already varies with respect to time. The POA irradiance which is feed in to the tool again gets multiplied by a factor to depict the variation of irradiance over the PV modules. For instance, if POA irradiance is $300W/m^2$, then 10% variation means that either $300W/m^2$ or $330W/m^2$ or $270W/m^2$, which is fed randomly across the PV modules. This results in stepped IV curves from the PV system caused by variation ranging from 0-20% that is fed. The valid configurations to be tested are selected based on the boundary conditions mentioned in the previous section. This configuration that is the number of PV modules in series (N_s) and PV modules in parallel (N_p) are tested one by one. For example, the valid PV module combinations for a 50kW system would be as follows,

- 2 Series, 84 Parallel
- 3 Series, 56 Parallel
- 4 Series, 42 Parallel
- 6 Series, 28 Parallel
- 7 Series, 24 Parallel
- 8 Series, 21 Parallel
- 12 Series, 14 Parallel

After this a simulink model of PV array shown in figure 5.1 was called in to the MATLAB script. The white blocks in the figure 5.1 is the PV module and is connected across to a variable voltage source (blue coloured box) to get the complete IV curve. The selected PV module was of Canadian Solar make with model number CS6K-300MS. It was a 60 cell 300Wp mono-crystalline silicon module, with 32.5V as V_{mpp} and 9.24A as I_{mpp} . There were 3 bypass-diodes in the module, each connected after every 20 cells connected in series. Each of the modules were modelled in Simulink model as per the available details from

the datasheet of selected PV module and then their connections in series and parallel were selected from the data input of MATLAB script. The input parameters such as POA irradiance and the calculated cell temperature was feed in the simulink model from the MATLAB script. In the simulink model, the various configurations of PV modules mentioned above for 50kW system can be simulated. Based on the input of number of modules in series and parallel, the appropriate configuration gets simulated. This simulink model returns the IV curve of the PV system based on the varying irradiance data provided to it.

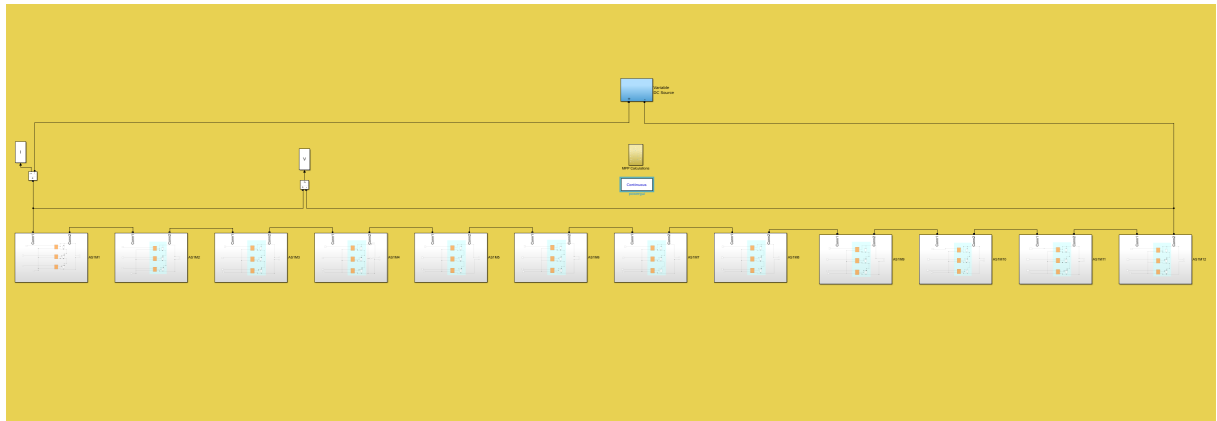


Figure 5.1: PV Simulink Model

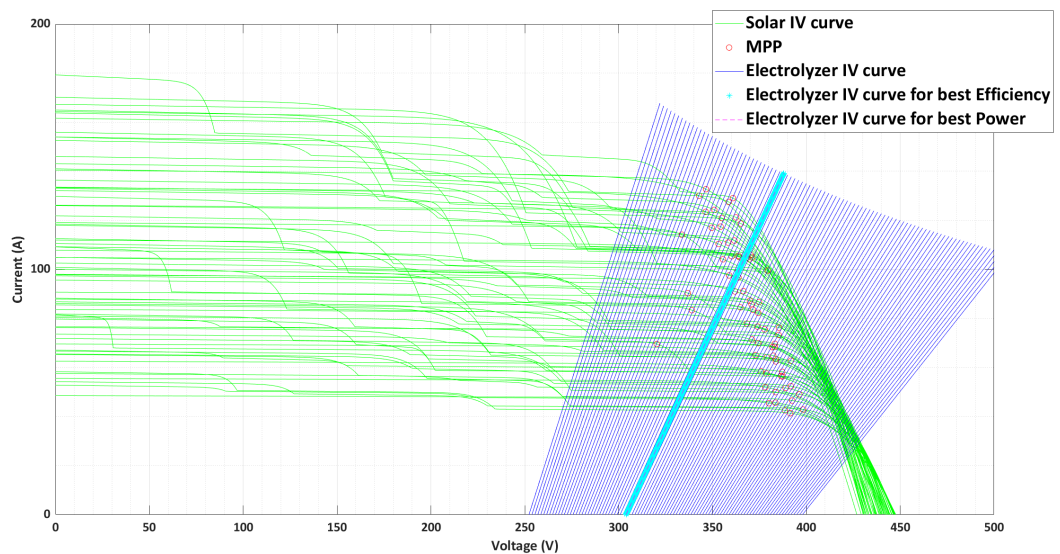


Figure 5.2: Electrolyzer IV curve's constraints

The number of cells inside the electrolyzer stack can vary between 1-250 based on the boundary conditions. As discussed in chapter 2, that we need to change the active area of cell while changing the number of cells in a single electrolyzer stack. This mainly to keep the capacity of electrolyzer in terms of kW constant. Therefore, it can be seen from figure 5.2 that the electrolyzer IV curves which are increasing in cell numbers along the right side of x-axis are also decreasing in height due to decreasing cell size and thus keeping a check of 50kW limit. It is clear that many of the 250 electrolyzer configurations available would be

very highly inefficient option for a selected configuration. In order to filter out, the electrolyzer curves which were very far from the MPP points of the selected IV curves of the PV system, few more constraints were set.

The constraints would be understood using an example for PV module configuration of 4 modules in series and 42 strings in parallel, that is used at STCA, Amsterdam. It is visible in the figure 5.2 that the set of electrolyzer IV curves for this configuration of PV configuration are not starting near the origin or 1.5556V which is the minimum extrapolated voltage for single cell electrolyzer's straight line IV curve. Rather it starts from 252V which corresponds to 162 cells in series in electrolyzer stack. The last IV curve also stops at 400V that is 257 cells in series inside the electrolyzer stack. For the lower limit or the first electrolyzer IV curve, the lowest V_{mpp} voltage from the pool of all possible MPP voltages for the selected PV configurations with all variations is selected. This lowest V_{mpp} value must be equal to the maximum voltage value for the selected IV curve of a electrolyzer configuration, to be the first curve under consideration. For the upper limit or the last electrolyzer IV curve, the voltage axis intercept of electrolyzer IV curve must be equal to highest value of V_{mpp} amongst the pool of all possible MPP voltages for the selected PV configurations with all variations. With these constraints applied, it ensures that all the MPP points come under the region of selected electrolyzer IV curves and also only electrolyzer IV curves closest to them are considered.

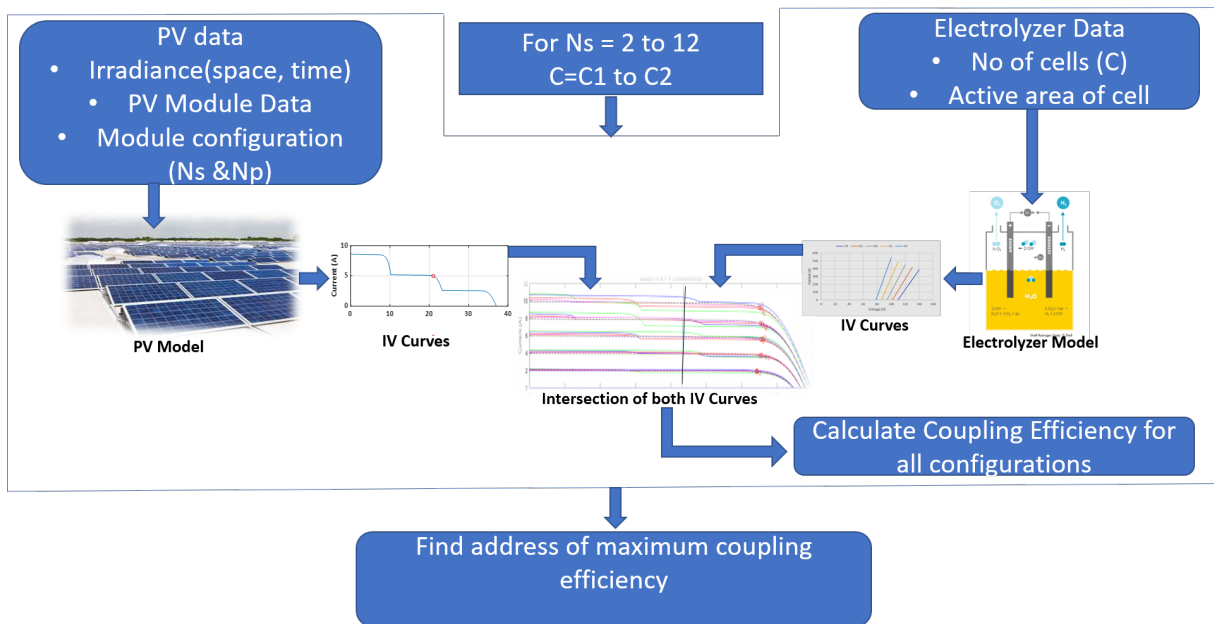


Figure 5.3: Logic for simulation

All this selection of electrolyzer curves happens using the MATLAB script. The intersection points of these IV curves from PV model and the electrolyzer model is calculated. Finally the coupling efficiencies are calculated once the intersections points or the operating power points are known. The whole logic is summarized in figure 5.3 which are as follows:

- First 2 modules are considered in series and rest in parallel
- Where the data needed for PV model in Simulink is fed and IV curves for PV system are obtained.
- Then the relevant configurations of electrolyzer are calculated.

combiner box and each row of modules with mounting structure took 2m of footprint. The pitch between each row was 1m. So, for all these cabling the specifications of cable provided by module manufacturer for module interconnection are sufficient as the maximum current for each one of them would short circuit current of the module. But after the combiner box were all the strings are connected parallel and the current adds up to a higher value. The combiner box was situated 25m away from the electrolyzer. For safety, the cables are required to be over designed by a factor of 1.56.

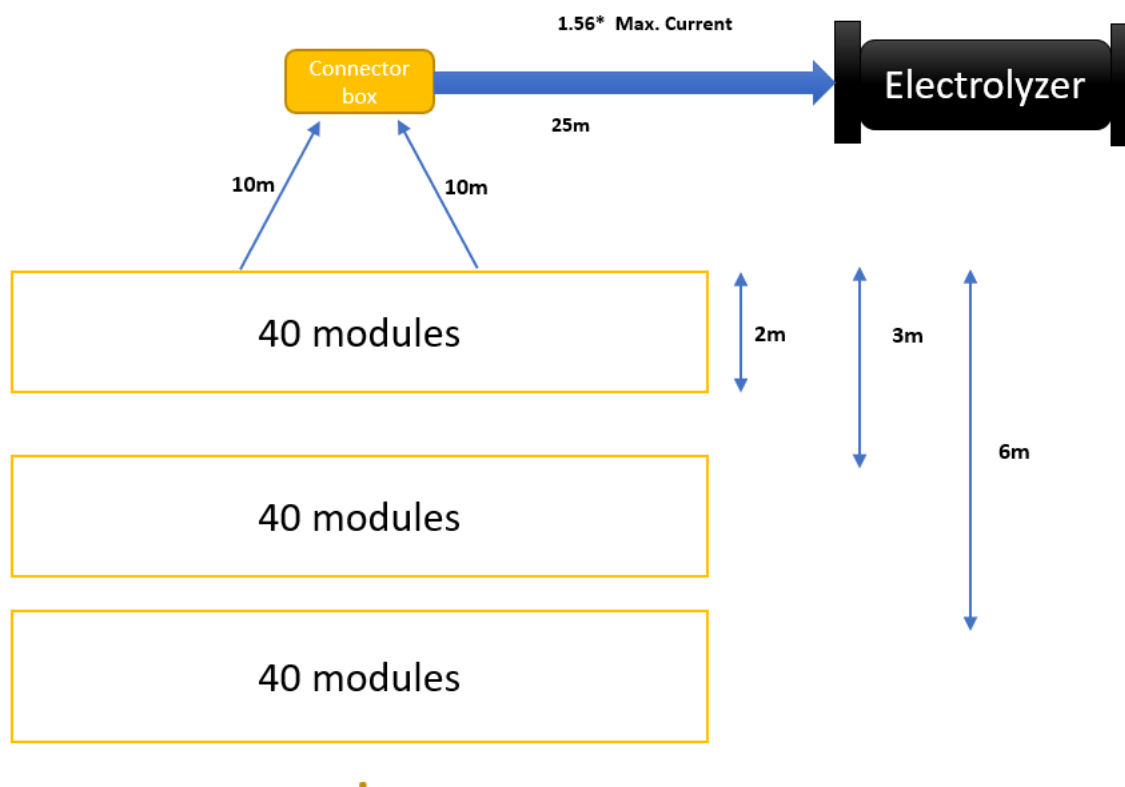


Figure 5.5: Simple layout of directly coupled system

5.2. Results for directly coupled system

In this section, the optimization method and results would be presented. First the time varying irradiance data was fed to the model and its results would be presented. Secondly the space varying irradiance would be fed to the model to resemble the combined effect of soiling, variations in module parameters and irradiance variation over the PV modules. In the third subsection the variation in coupling efficiency with different months would be understood. Finally for all the conditions the effect of excluding the ohmic resistance would be presented.

5.2.1. Performance of directly coupled system with time varying irradiance

The daily irradiance profile for any place on earth can be represented by figure 5.6, which is a bell curve with peak during the mid day. The yellow box in the figure shows the peak

irradiance period during the noon time. This is the GHI irradiance received on a plane parallel to ground. The irradiance keeps on varying within the span of a day. To start with, hourly average irradiance for the month of July in Amsterdam was considered. This weather data was taken from Meteonorm's database. This GHI irradiance was converted into POA irradiance which is different for east facing and west facing modules.

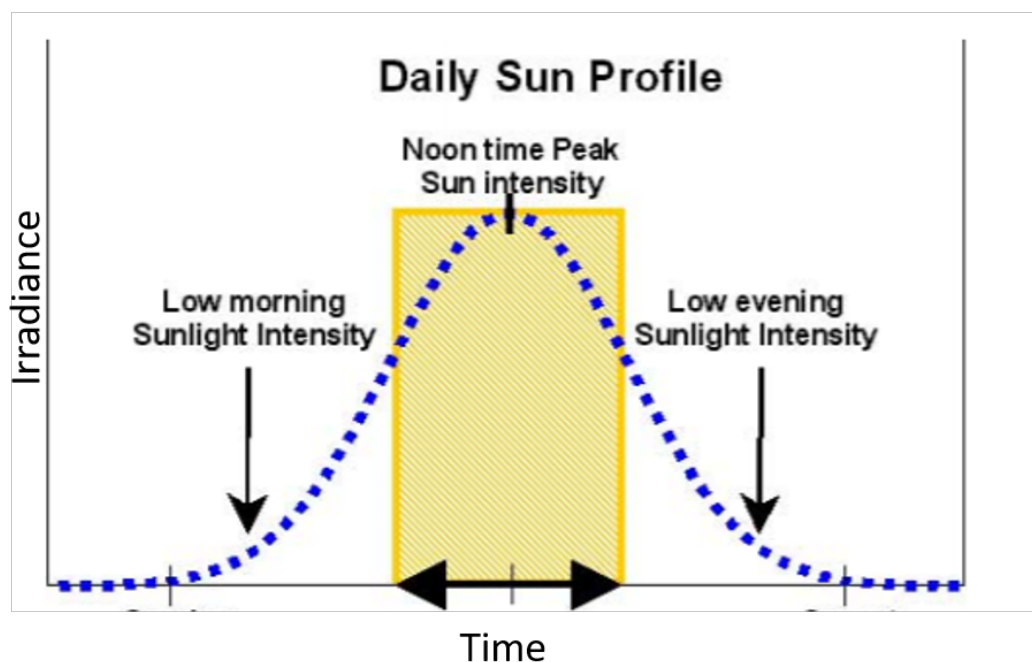


Figure 5.6: Daily Irradiance Profile, (Balafas et al., 2010)

The optimization was performed using this irradiance data and the outcome was shown in figure 5.7. The best configuration was 3 PV modules in series and 56 such strings in parallel. It should be connected with electrolyzer of 52 cells in series with active area of 1154cm^2 per cell. This configuration gives 99.83% efficiency even with varying irradiance, which confirms high utilization of available power from PV system. The best configuration of electrolyzer is highlighted by cyan blue colour in the graph.

The most efficient option was expected for a configuration with fewer PV modules in string. It is mainly due to the fact that the MPP's of PV systems are aligned more in a straight line for such configurations as shown in 5.8. The electrolyzer curve also straightens as we move towards the left on voltage axis. As we move towards the right, the electrolyzer curve's slope decreases and the intersection points spread away from the MPP points. Though there is a global optimum for the most efficient configuration but it is possible that the configuration for that particular type of electrolyzer is not possible. It maybe difficult to procure electrolyzer cells and membranes of specific diameter for an electrolyzer. Therefore there is a need to see how much is compromised while shifting towards the next optimum configuration.

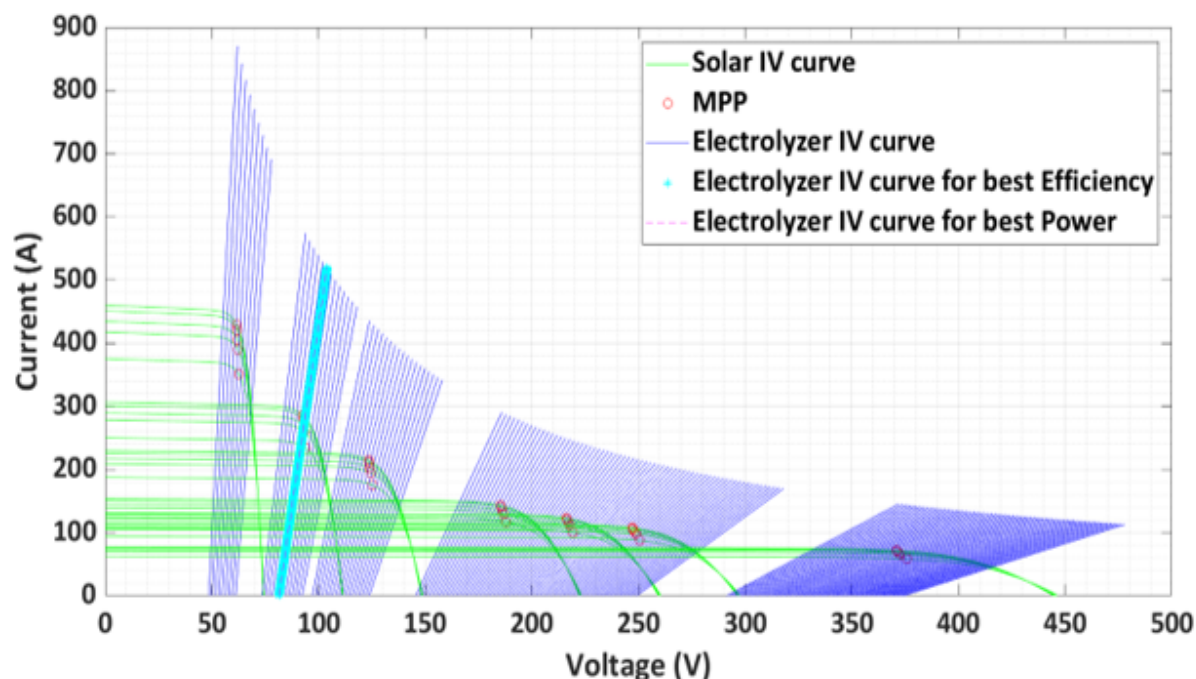


Figure 5.7: IV curves of all possible configurations

As shown in figure 5.9, the coupling efficiency ranges between 99.74% and 99.83%. In this graph the coupling efficiency for all the PV string length is given. The corresponding electrolyzer configuration can be found as well. Then the user can pick the desired configuration as per the availability in the market. In this case where the irradiance variation and module parameter variation is considered zero, the maximum difference between the highest and lowest efficiency from figure 5.9 is 0.9%. With this compromise you can choose the any of the string length of PV and its corresponding electrolyzer for best efficiency.

From the yearly irradiance data from the physical setup, the total energy production can be estimated to 29Mwh for the 50kW system. Out of this available energy, almost 28.4Mwh can be extracted from the PV-electrolyzer coupling after optimizing the efficiency to 98.83%. It was seen that around 0.9% compromise can be done to select other configurations, which would result in loss of 295kWh of energy and 50 Euros per year @ 0.17Euros/kWh.

5.2.2. Change in coupling efficiency with inclusion of space varying irradiance

The coupling efficiency is effected when we add variation in irradiance falling on each module. The variation is also depicting the effect caused by varying soiling over modules and varying module parameters due to non uniformity during manufacturing or defects post use. All the effects combined can range upto 20% in worst case due to multiple module failure or replacements with higher rated modules. In this sections all the irradiance will be fed into to the module first without variation and then four more times again with 5, 10, 15 and 20% variation.

With a small 5% variation in irradiance falling on each modules randomly, the following outcome was available as shown in the figure 5.10. The small steps on IV curves of PV is visible due to the introduced variation. The shortest string configuration of PV i.e 2 modules in a string and 84 such strings in parallel gave the best efficiency of 97.93% for

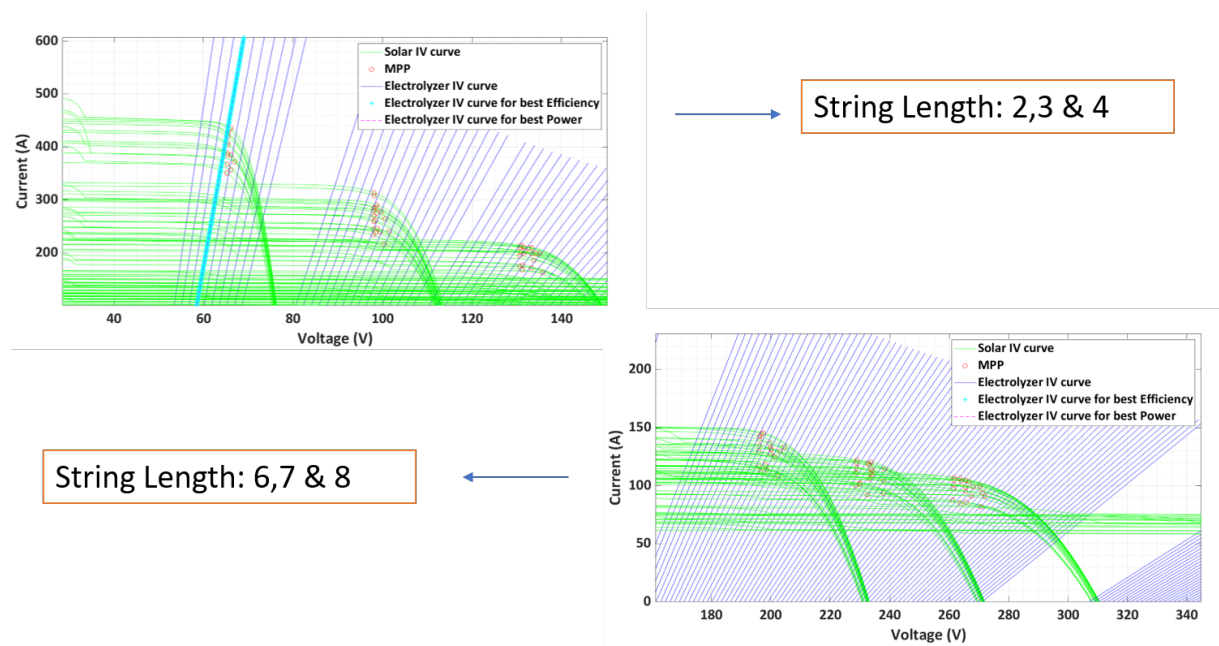


Figure 5.8: Closeup of all IV curves

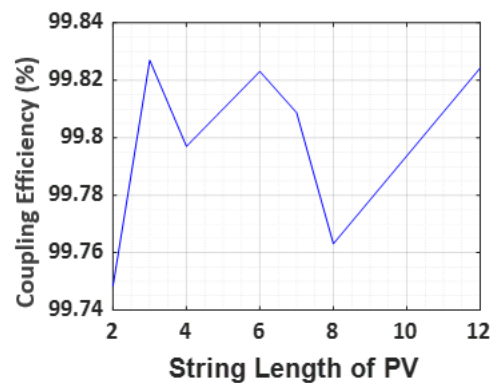


Figure 5.9: Deviation in Coupling Efficiency

the first iteration. The most suited electrolyzer model with it was 35 number of 1715cm^2 active area cells in the stack. In the second iteration the best configuration changed to 7 panels in string with efficiency of 98.16%, as seen in figure 5.11. These changes in optimum efficiencies are due to the randomized input of irradiance to the PV array. The maximum difference between efficiencies of any two configuration from figure 5.11 is 1.25%.

A maximum of 1.25% compromise in efficiency would be required in this case, if the least optimum amongst the local maximas is to be chosen instead of the global maxima. This 1.25% compromise can result into 362.5kWh of energy loss annually. The 362.5kWh energy loss will result into 61.6 Euros loss annually @ 0.17Euros/kWh

The whole optimization was performed once without the inclusion of the ohmic losses. It can be seen in figure 5.12, the shorter string lengths performance without the ohmic losses gives efficiency above 99%. This is an over-estimate due to ignoring of ohmic losses. The

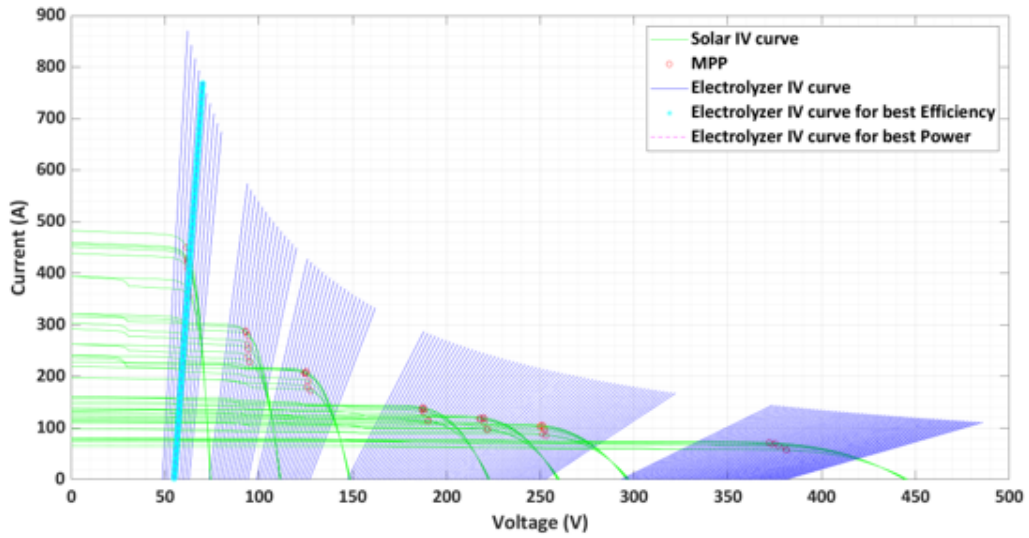


Figure 5.10: IV curves of all possible configurations with 5% variation

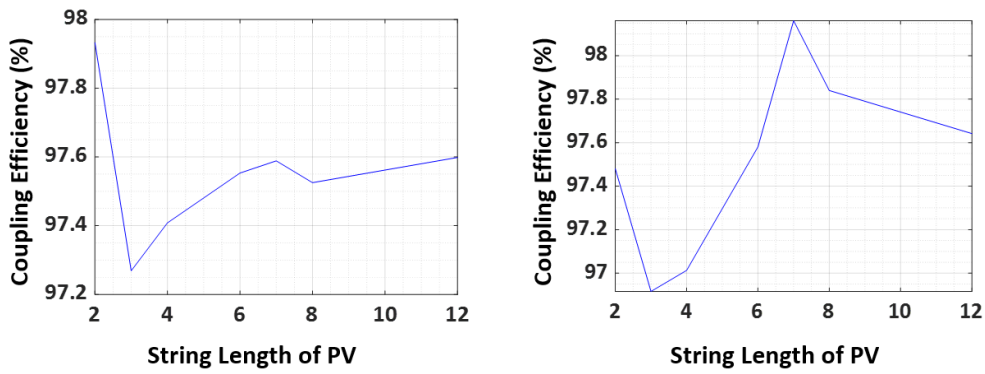


Figure 5.11: Difference in Coupling Efficiency with 5% variation

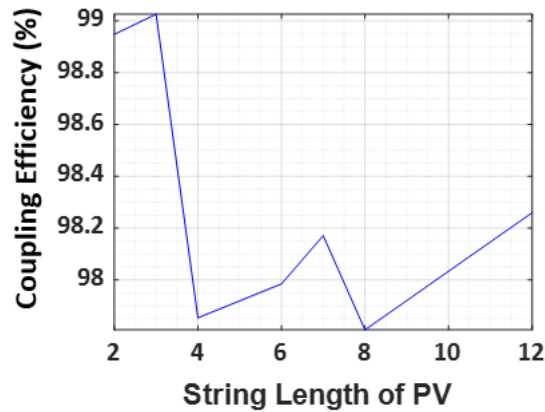


Figure 5.12: Without considering the ohmic loss

ohmic losses were calculated for cables selected just within the safe range. The losses can be reduced by spending more by using thicker cables for shorter string length configurations.

We keep on adding the variations and test the changes, with 10% variation not much has changed with the best configuration. As shown in figure 5.13, the best configuration is 2 cells in series and 84 of such strings in parallel connected to 37 cells electrolyzer stack each with active area of 1621cm². The shorter string length remains to be the best configuration yet with 10% variations with efficiency of 96.54%. But the efficiency has surely dropped below 97% which is a bit lower than the efficiencies we got for 5% variation case.

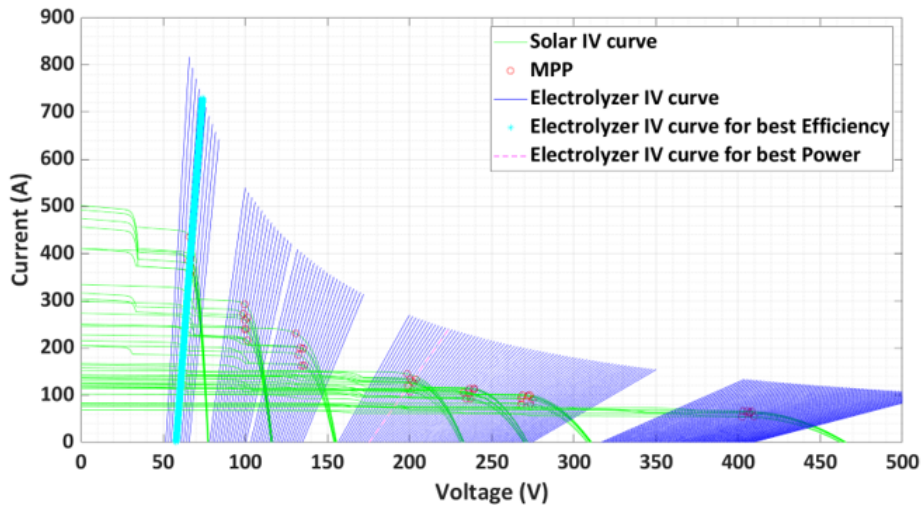


Figure 5.13: IV curves of all possible configurations with 10% variation

A maximum difference of 3% is present amongst the local maxima's of different configuration, which means a energy loss of 870kWh annually. This corresponds to 148 Euros lost which is 2.96 Euros/kWp. This loss at GW scale would be a bigger blow of 2.96 million euros for 1 GW plant. It now justifies the extent upto which the variations can cause the damage. Now for 15% variation applied the best configuration again remained the same but the optimum coupling efficiency dropped to 96.43%. The coupling efficiencies varied between 89% and 96%, giving a maximum difference of 7% in efficiencies as shown in figure 5.14. This would result in 2030kWh energy loss and 345 Euros per year revenue loss which is 7 Euros/kWp. One more thing that can be observed is that the ohmic losses are becoming more significant with increasing variations. We can see from figure 5.15, the coupling efficiency is over-predicted for shorter string length by almost upto 6%.

Similarly for higher variations above 15%, the best configuration remains the same. The remaining graphs are provided in appendix A1. For the bigger strings the efficiency drops rapidly as the variation increases. The significance of considering ohmic losses also increases with increasing variations. As it causes over prediction of efficiency and thus the power production. It can be seen in figure 5.16, the addition of ohmic losses shifts the lower efficiency regions to the left. The highest effect is visible on the lower string lengths, as they have higher currents. But until 10% variation in irradiance or module parameter is observed, there is no significant change in coupling efficiency.

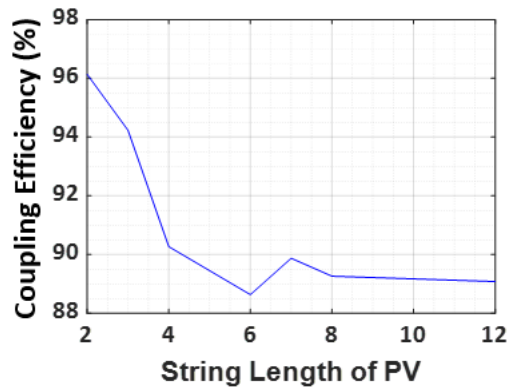


Figure 5.14: Difference in Coupling Efficiency with 15% variation

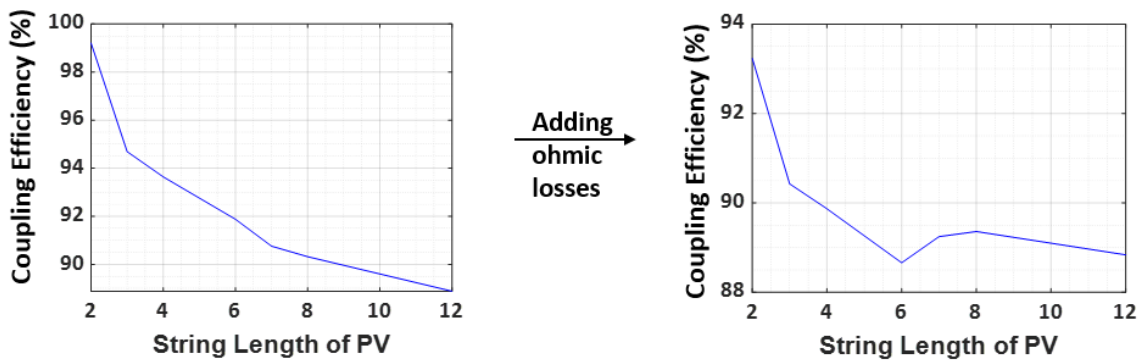


Figure 5.15: Effect of adding ohmic losses

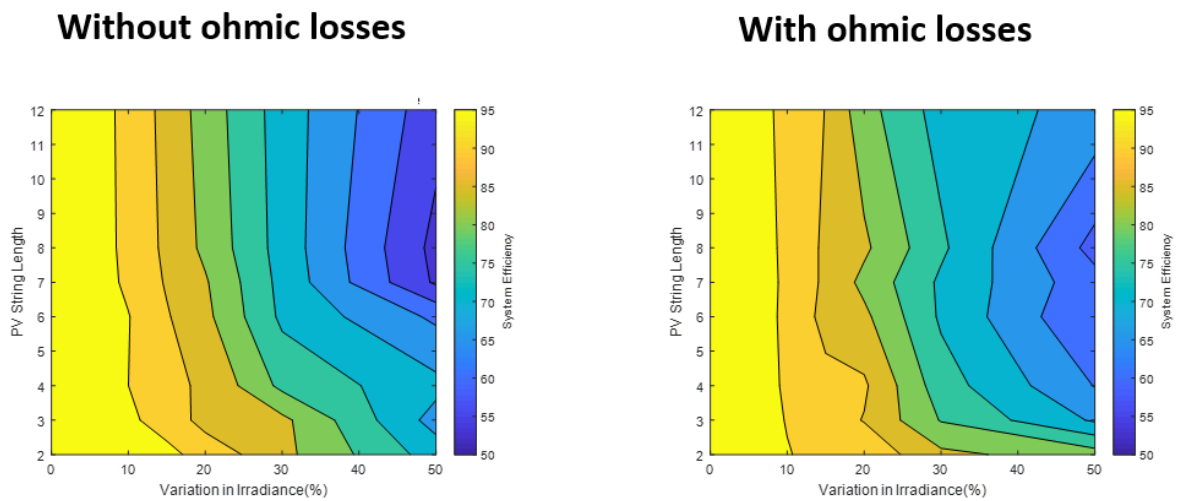


Figure 5.16: Heatmap showing the effects of including ohmic losses

5.2.3. Variation in coupling efficiency with months

It is also desirable to know the variation in coupling efficiency month-wise or season-wise for the selected configuration. Hourly irradiance data for each month was taken from the

KNMI database, who has a weather station in Schipol, Amsterdam.

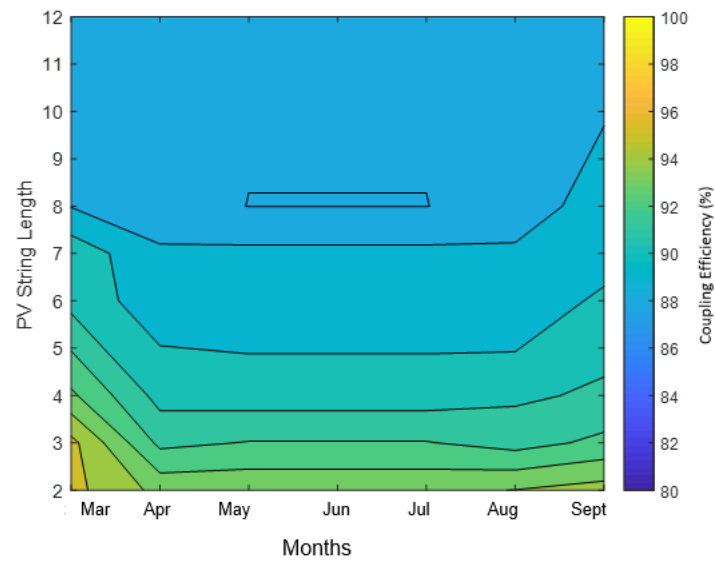


Figure 5.17: Month wise variation in efficiency

The irradiance values above 350 W/m^2 were used, as it is the lower limit for the electrolyzer to start. Only 7 months were able to contribute to the hydrogen production which had sufficient irradiance. The figure 5.17, shows the coupling efficiencies for each PV string configuration for every month on X axis. The months from April to August contribute to the maximum sun hours in the year. The coupling efficiency is mostly above 90% for all short string lengths. For higher string lengths above 10, causes the efficiency to hover between 86 and 84%. So, in general the shorter string lengths connected with lesser but bigger electrolyzer cells are the best configuration.

6

Power converters & transformers in DC-AC-DC configuration

A second configuration which needs to be tested for PV-electrolyzer system is the DC-AC-DC system. When the PV system and the electrolyzer is to be installed significantly further apart from each other, the directly coupled system would be disadvantaged due to ohmic losses. A simplified layout for this type of connection is shown in the figure 6.1. The PV system is connected to the inverter, which has a MPP tracking system embedded inside it. Irrespective of the series parallel configuration of PV modules, the MPP tracker makes the PV system work near its MPP. Usually the MPP tracker's efficiency is mostly over 98%. The inverter converts the DC power into AC and feeds it to the transformer. The first transformer steps up the voltage and reduces the current to a level where ohmic losses get minimized. Here it can be connected to a transmission line which can take the cables km's away towards the electrolyzer. The voltage needs to be stepped down again using a transformer and then fed into a rectifier. This rectifier will convert the AC power back to DC before supplying it to the electrolyzer.

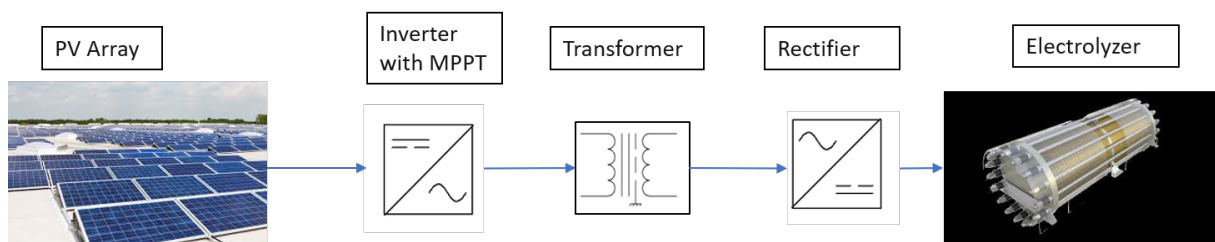


Figure 6.1: DC-AC-DC configuration

By converting the power into AC the following are the advantages,

- We can extract maximum power of PV system using MPP trackers inside the Inverters.
- The ohmic losses maybe equal or lesser than the direct coupling's transmission losses.
- Using green power from distant location is possible for electrolysis.
- Once transformed to AC, the grid can be used for stabilizing the PV-Electrolyzer system.

The main disadvantage that comes is the requirement of either a storage device or grid for balancing of power in case we use some device like phase angle controller. The second option would be using a sophisticated control at either of the converters to maintain the operating

voltage and current before the electrolyzer. This would ensure that the input voltage and current fed are always lying on the electrolyzer IV curve else the electrolyzer would not operate. Though the ohmic losses are curtailed using step up transformers but the multiple components added come with their own efficiencies. The power electronics and transmission systems have been developed a lot over time resulting into high efficiencies.

6.1. Varying DC-AC-DC configuration efficiency

The efficiency of these components vary with respect to the connected load and the applied input voltages, which would be explained in this section further.

6.1.1. Efficiency variation of inverters

Inverter is simply a power electronic converter used for converting DC power into AC power. Usually PV inverters are used to connect the PV farms to the grid which is a AC transmission line, where the maximum power is extracted using the MPP algorithms inside the inverters and delivered to the grid. It also acts like a protection device where it shuts down in-case of high short circuit current. There are inbuilt filters in inverters for stabilizing the output power. The inverter considered for this study is of SMA make. It is a 50kW inverter with MPP tracking in the range of 300V to 480V.

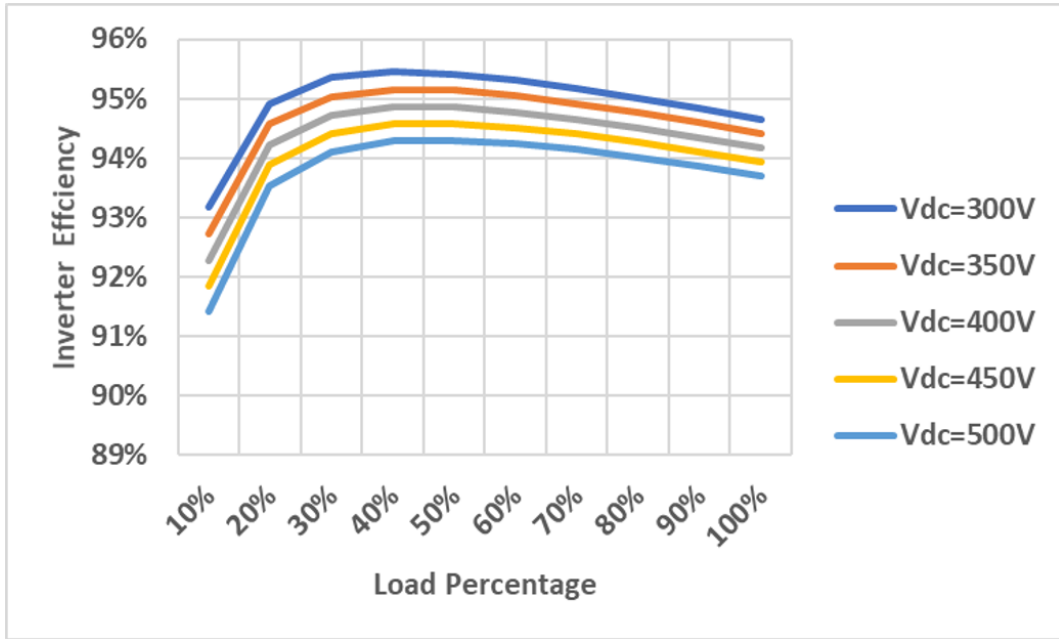


Figure 6.2: Varying inverter efficiency

The varying SNL efficiency model for inverter was given by (King et al., 2007). The SNL model describes the performance of inverter at varying load percentages and input voltages. The efficiency is given by the following equations:

$$P_{ac} = \{(P_{aco}/(A - B)) - C \cdot (A - B)\} \cdot (P_{dc} - B) + C \cdot (P_{dc} - B)^2 \quad (6.1)$$

$$A = P_{dco} \cdot \{1 + C_1 \cdot (V_{dc} - V_{dco})\} \quad (6.2)$$

$$B = P_{so} \cdot \{1 + C_2 \cdot (V_{dc} - V_{dco})\} \quad (6.3)$$

$$C = C_0 \cdot \{1 + C_3 \cdot (V_{dc} - V_{dco})\} \quad (6.4)$$

Where C_0 , C_1 , C_2 and C_3 are coefficients which vary with the inverter model. While P_{ac} is the ac-power output, P_{dc} is the dc-power input, V_{dc} is the dc-voltage input, P_{aco} is maximum ac-power at the reference conditions, P_{dco} is the dc-power at reference conditions, V_{dco} is the reference dc-voltage conditions and P_{so} is dc-power used by inverter. The variation in efficiency of inverters is shown in figure 6.2. The efficiency is low when the load is below 20% of its maximum load, the efficiency drops rapidly. Post 20% it increases and stabilizes at almost a constant value of efficiency. Ususally, the inverter efficiencies are above 97-98% these days. The inverter needs to have a smaller MPPT tracking range in this case and these type of inverters are lower in efficiency in the range of 94-95%. The MPPT efficiency is not included in this model and mostly the new algorithms used give tracking efficiencies above 98%.

6.1.2. Efficiency variation of transformers

A transformer is device used for stepping up or stepping down the voltage which enables transmission with reduced ohmic losses. The efficiency for transformer varies in similar fashion to that of inverter as shown in figure 6.4. A 75kVA transformer was selected of Schneider make, with model number EX75T3HCU. The rated efficiency of transformer at 35°C was 98.7% which with copper winding.



Figure 6.3: Transformer

The efficiency of transformer is given by the following equations:

$$\% \text{ Efficiency} = \frac{100 \times P \times VA}{(P \times VA) + \text{Core Loss} + (P^2 \times \text{coil Loss XT})} \quad (6.5)$$

In the above equation P refers to the fraction of total load and VA refers to the full load. The transformer selection was done in a way that the maximum efficiency of transformer is where the load values occurs the most. From the figure 6.4, it is visible that the STCA

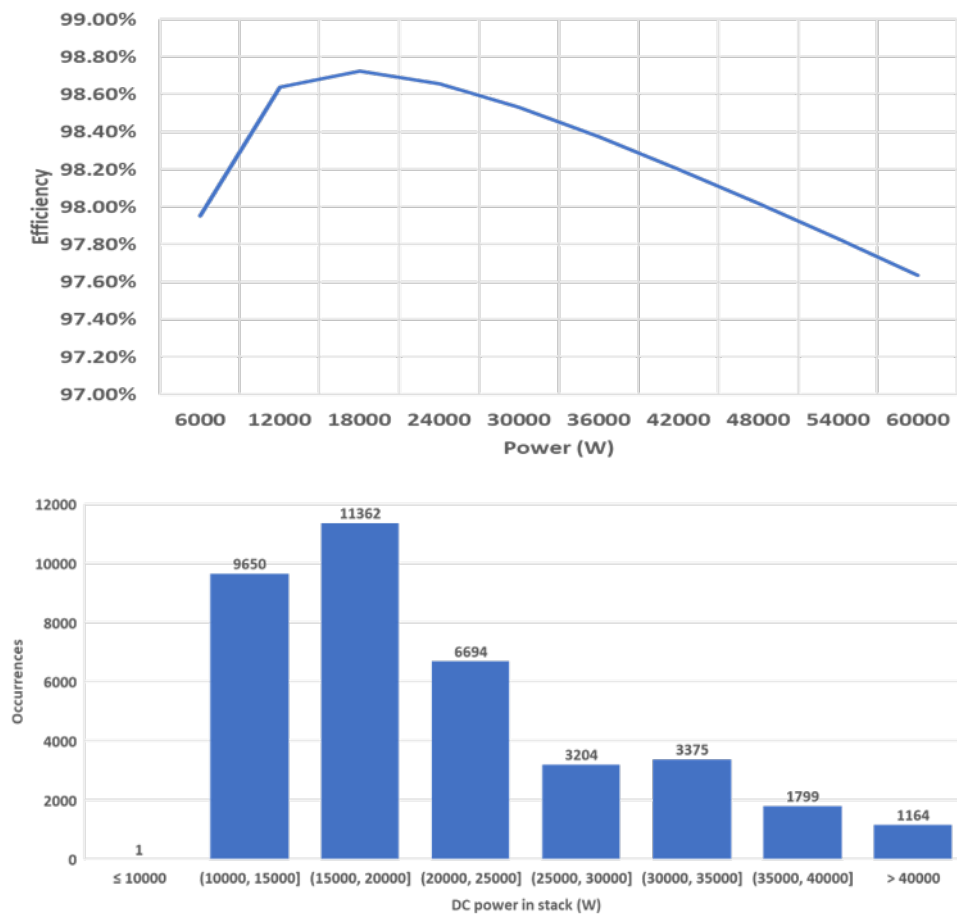


Figure 6.4: Varying efficiency of transformer

DC-AC-DC Efficiency		
Sr. no.	Components	Efficiency
1	MPPT	0.99
2	Inverter	0.94 - 0.96
3	Step down - Transformer	0.97-0.99
4	Rectifier	0.98
5	Cabling (deducting Ohmic losses)	varying

Figure 6.5: Efficiencies of each component

system worked in the region of 15kW -20kW for most part of the year and correspondingly the transformer efficiency at this load is the highest.

the MPPT efficiency was considered constant at 99%, as there is no data available for it

from the manufacturer. The efficiency for rectifier was kept constant as well at 98%, but in reality it will vary as well. Finally the efficiencies of each component is concluded in the figure 6.5.

6.2. Comparison of DC-AC-DC and direct coupling configuration

Finally both the configurations of directly coupled system and the DC-AC-DC systems are compared together. The figure 6.6, shows the varying coupling efficiency with changing irradiance and applied variations in irradiance. It is visible that for directly coupled system, most part of the heatmap is yellow in colour which represents highest efficiency range of 95-99%. While on the other hand DC-AC-DC configuration gives efficiencies between 85-89%. There is a clear gap of around 5-10% between their efficiencies. This is majorly due to additional components adding up to the total coupling efficiencies. The results mean 1450-2900kWh energy is lost which translated to a loss of 246-493 Euros or 4.93-9.86 Euros/kWp.

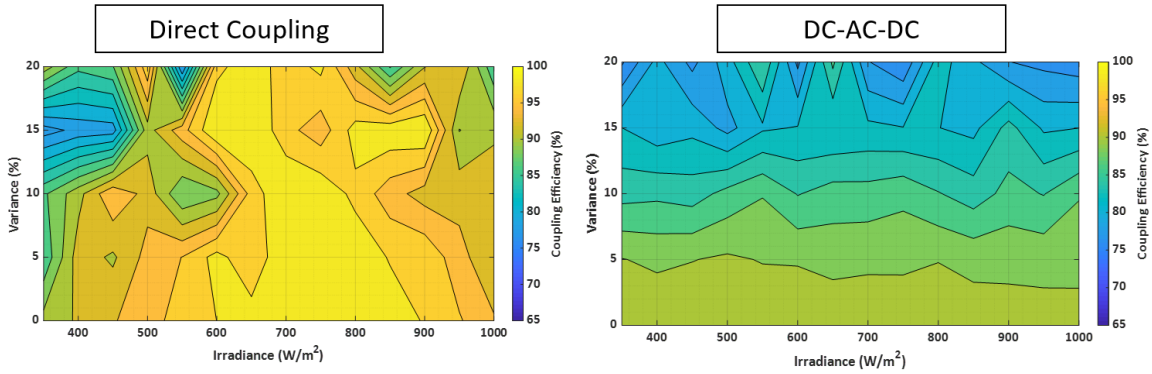


Figure 6.6: Comparison of varying efficiency between directly coupled and DC-AC-DC

During the higher irradiance range ($700-900\text{W}/\text{m}^2$) the directly coupling without any variations is clearly leading by 10% in efficiency. Now we focus only on $200-700\text{W}/\text{m}^2$ region, from where the most energy comes as per figure 4.17. At lower irradiances this gap between the efficiencies of two configuration reduces. The variance in irradiance or the deterioration of modules may bring decrease in efficiencies of direct coupling but the decrease in efficiencies for DC-AC-DC configuration is even more. This is without any consideration for deterioration of power electronic components in DC-AC-DC configuration.

6.2.1. Weighted efficiencies of directly coupled and DC-AC-DC configurations

As we know each of the irradiance brackets contribute differently towards the energy production using the respective configurations. Therefore each irradiance bracket was given weights based on their occurrences and contribution to the power production. The percentages are written above the histograms in the figure 6.7 and inside them are the occurrences of each irradiance brackets throughout the year. These weights are as per the irradiance data for Amsterdam, similarly for other cities it can be calculated using the weather database. The weighted efficiency for both the configuration in Amsterdam is given by the following equation:

$$\begin{aligned}
 \eta_{wt} = & 15.77\% * \eta_{350-400} + 12.03\% * \eta_{400-450} + 12.49\% * \eta_{450-500} + 11.39\% * \eta_{500-550} \\
 & + 9.024\% * \eta_{550-600} + 9.39\% * \eta_{600-650} + 9.57\% * \eta_{650-700} + 6.56\% * \eta_{700-750} \\
 & + 7.02\% * \eta_{750-800} + 4.1\% * \eta_{800-850} + 2.37\% * \eta_{850-900} + 0.18\% * \eta_{900-950} \\
 & + 0.0911\% * \eta_{950-1000}
 \end{aligned} \tag{6.6}$$

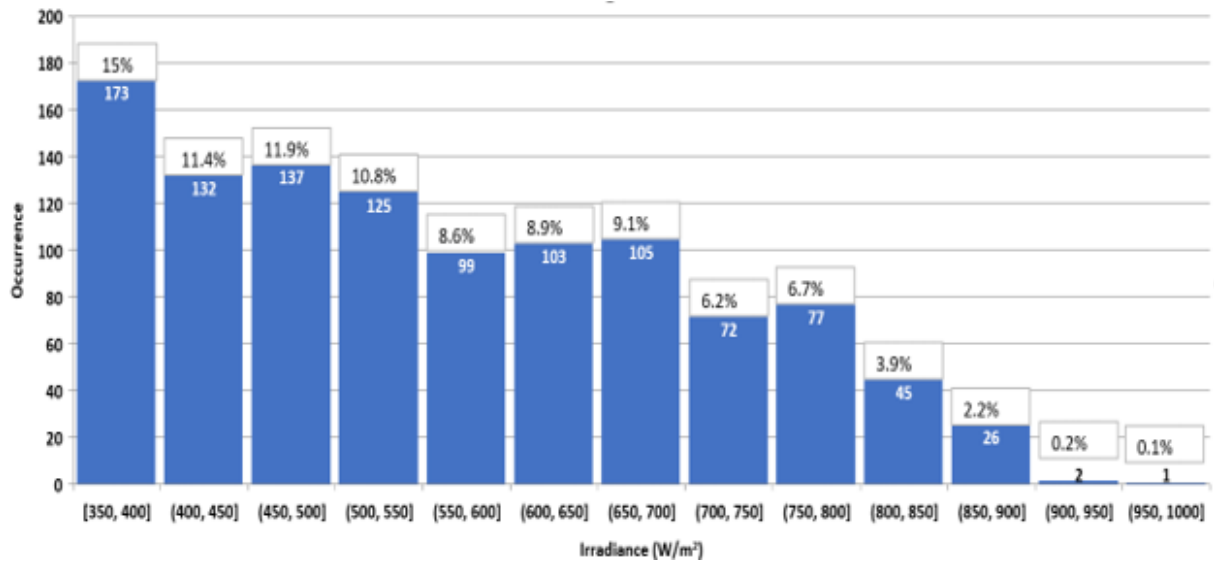


Figure 6.7: Occurrences of each irradiance bracket at STCA in 2019-2020

For directly coupled systems this weighted efficiency turns out to be 95.7% and for the DC-AC-DC configuration it was 90.63%.

7

Conclusion

The research was started with the intent to know much more in detail about the direct coupling configuration. We wanted to understand the boundary conditions needed while designing the directly coupled system, which were set using the data from the setup of electrolyzer and literature study. A tool was developed to optimize PV-electrolyzer directly coupled system. The variations of irradiance and module parameters on the system which was not observed by any one in the literature was accomplished in this study. A new configuration of DC-AC-DC for PV-electrolyzer system was compared to the existing directly coupled system. In the following paragraphs a brief overviews of all this accomplishments of the research questions would be discussed.

Based on the comments from industrial experts, the boundary limitations were set for this tool, like no configuration that breaches 500V limit should be simulated. No literature based on this limit is available but it can be speculated that occurrence of non-uniform degradation amongst the electrolyzer cells could be the reason for this set limit. The lower limit of 35% was set to start the PV-electrolyzer system, as below this limit cross over of hydrogen takes place. Correspondingly, the irradiances below $350\text{W}/\text{m}^2$ were hence neglected. The ohmic losses had an impact on short string length configuration like 2 or 3 or 4 PV modules in series, which was again visible after 10% variation was introduced in the input parameters.

A tool was developed in MATLAB-Simulink to simulate the best configuration for PV-electrolyzer directly coupled system. The electrolyzer cells are available in different sizes in the market and could be even modified for large scale projects based on feasibility. Therefore in this study the cell sizes of electrolyzers were changed with number of cells per electrolyzer stack to find the best match corresponding to a particular PV configuration. From the tool it was clear that the smaller string length of PV combined with bigger but lesser number of electrolyzer cells in stack gave the best efficiency. The output shows for the above mentioned configuration efficiency in the range of 90-95% efficiency could be achieved even with a variation of 20% caused by space varying irradiance, module parameters, soiling etc or the seasonal variations. Upto 10% variation scenario, the other best configuration provided could be used with a maximum compromise of 3% in coupling efficiency and hence the other comparatively a bit less efficient configurations could be selected as per module availability. That loss corresponded to 870kWh energy loss per year for a 50kWp system. Economically this results into 148 Euros or 2.96 Euros/kWp loss. This may seem a small number at kW scale but at 1 GW scale it will result into a loss of 2.96 million Euros. So it is important

to consider these variation that may be caused due to non uniformity in modules, varied soiling loss or space varying irradiance.

In comparison to the DC-AC-DC configuration, directly coupled gave a better additional efficiency of 5-10% due to the absence of additional power electronic components. Direct Coupling gives a weighted efficiency of 95.7% for Amsterdam, while DC-AC-DC configuration gives 90.63%, considering variation 0-5%.

7.1. Recommendations

There are a few more things that can answered pertaining to the field of PV-Electrolyzer system such as:

- Modelling and testing of DC-DC converter topology for hydrogen generation from PV.
- DC-AC-DC system could be manufactured at lab scale and tested for its robustness and efficiency.
- A feasibility study is required for the bigger cell size electrolyzer using CFD analysis as it could big hotspot issues.
- Simulations must be repeated post getting the data for DHI and DNI reading from the new apparatus installed.
- A more sophisticated model that includes the performance variation of electrolyzer due to temperature is needed.

Bibliography

- Aki, H., Sugimoto, I., Sugai, T., Toda, M., Kobayashi, M., and Ishida, M. (2018). Optimal operation of a photovoltaic generation-powered hydrogen production system at a hydrogen refueling station. *International Journal of Hydrogen Energy*, 43(32):14892–14904.
- Balafas, C., Athanassopoulou, M., Argyropoulos, T., Skafidas, P., and Dervos, C. (2010). Effect of the diffuse solar radiation on photovoltaic inverter output. In *MELECON 2010-2010 15th IEEE Mediterranean Electrotechnical Conference*, pages 58–63. IEEE.
- Carmo, M., Fritz, D. L., Mergel, J., and Stolten, D. (2013). A comprehensive review on pem water electrolysis. *International journal of hydrogen energy*, 38(12):4901–4934.
- Chisholm, G. and Cronin, L. (2016). Hydrogen from water electrolysis. In *Storing Energy*, pages 315–343. Elsevier.
- Clarke, R., Giddey, S., Ciacchi, F., Badwal, S., Paul, B., and Andrews, J. (2009). Direct coupling of an electrolyser to a solar pv system for generating hydrogen. *International journal of hydrogen energy*, 34(6):2531–2542.
- Commission, E. (2020). A hydrogen strategy for a climate neutral europe. <https://bit.ly/2ZWryv1>. Accessed: 2020-7-9.
- Cook, J., Nuccitelli, D., Green, S. A., Richardson, M., Winkler, B., Painting, R., Way, R., Jacobs, P., and Skuce, A. (2013). Quantifying the consensus on anthropogenic global warming in the scientific literature. *Environmental research letters*, 8(2):024024.
- de Fátima Palhares, D. D., Vieira, L. G. M., and Damasceno, J. J. R. (2018). Hydrogen production by a low-cost electrolyzer developed through the combination of alkaline water electrolysis and solar energy use. *International Journal of Hydrogen Energy*, 43(9):4265–4275.
- de Laat, P. (2020). Overview of hydrogen projects in the netherlands. <https://www.topsectorenergie.nl/sites/default/files/uploads/TKI%20Gas/publicaties/Overview%20Hydrogen%20projects%20in%20the%20Netherlands%20versie%201mei2020.pdf>. (Accessed on 08/13/2020).
- Djafour, A., Matoug, M., Bouras, H., Bouchekima, B., Aida, M., and Azoui, B. (2011). Photovoltaic-assisted alkaline water electrolysis: Basic principles. *international journal of hydrogen energy*, 36(6):4117–4124.
- Dönitz, W. and Erdle, E. (1985). High-temperature electrolysis of water vapor—status of development and perspectives for application. *International Journal of Hydrogen Energy*, 10(5):291–295.
- Duc, T. N., Goshome, K., Endo, N., and Maeda, T. (2019). Optimization strategy for high efficiency 20 kw-class direct coupled photovoltaic-electrolyzer system based on experiment data. *International Journal of Hydrogen Energy*, 44(49):26741–26752.
- Europe, H. (2020). Hydrogen in industry. <https://bit.ly/30TT6U7>. Accessed: 2020-6-18.
- García-Valverde, R., Espinosa, N., and Urbina, A. (2011). Optimized method for photovoltaic-water electrolyser direct coupling. *international journal of hydrogen energy*, 36(17):10574–10586.
- Hansen, C. W. (2020). Parameter estimation for single diode models of photovoltaic modules. <https://prod-ng.sandia.gov/techlib-noauth/access-control.cgi/2015/152065.pdf>. Accessed: 26-07-2020.
- Ibrahim Dincer, A. A. (2018). Electrolyzers. In *Comprehensive Energy Systems*,. Elsevier.

- IEA (2020a). Announced wind and solar pv average auction prices by commissioning date. <https://bit.ly/2AJatfE>. Accessed: 2020-6-18.
- IEA (2020b). Explore energy data by category, indicator, country or region. <https://bit.ly/2Z0AG1B>. Accessed: 2020-6-18.
- Industries, M. H. (2020). Hydrogen the next step in energy evolution. <https://bit.ly/324gjnd>. Accessed: 10-07-2020.
- IRENA (2019). Hydrogen: A renewable energy perspective. <https://bit.ly/2W2UikO>. Accessed: 2020-6-18.
- Jeffrey R. S. Brownson (2020). 4.4 empirical correlation for estimating components of light | eme 810: Solar resource assessment and economics. <https://www.e-education.psu.edu/eme810/node/683>. (Accessed on 08/14/2020).
- King, D. L., Gonzalez, S., Galbraith, G. M., and Boyson, W. E. (2007). Performance model for grid-connected photovoltaic inverters. Sandia National Laboratories SAND2007-5036.
- Kovač, A., Marciuš, D., and Budin, L. (2019). Solar hydrogen production via alkaline water electrolysis. *International Journal of Hydrogen Energy*, 44(20):9841–9848.
- Laboratories, S. N. (2020). Single diode equivalent circuit models. <https://pvpmc.sandia.gov/modeling-steps/2-dc-module-iv/diode-equivalent-circuit-models/>. Accessed: 25-07-2020.
- Laoun, B., Khellaf, A., Naceur, M. W., and Kannan, A. M. (2016). Modeling of solar photovoltaic-polymer electrolyte membrane electrolyzer direct coupling for hydrogen generation. *International Journal of Hydrogen Energy*, 41(24):10120–10135.
- Loudenback, T. and Jackson, A. (2018). The 10 most critical problems in the world, according to millennials. <https://bit.ly/2Oahj0T>. Accessed: 2020-6-18.
- Maeda, T., Nagata, Y., Endo, N., and Ishida, M. (2016). Effect of water electrolysis temperature of hydrogen production system using direct coupling photovoltaic and water electrolyzer. *Journal of International Council on Electrical Engineering*, 6(1):78–83.
- Maroufmashat, A., Sayedin, F., and Khavas, S. S. (2014). An imperialist competitive algorithm approach for multi-objective optimization of direct coupling photovoltaic-electrolyzer systems. *International journal of hydrogen energy*, 39(33):18743–18757.
- Martin, J. (2020). Stca solar pv and electrolyser direct coupling pilot: Part 2. Shell Internal Report.
- MathWorks (2020). Simulink - simulation and model-based design - matlab & simulink. <https://nl.mathworks.com/products/simulink.html>. (Accessed on 08/07/2020).
- Nel (2019). Hydrogen technology innovations. <https://bit.ly/2Dm0Fcl>. Accessed: 09-07-2020.
- Nepal, P. (2018). Effect of soiling on the pv panel kwh output. Accessed: 05-08-2020.
- Paul, B. (2009). Direct coupling of the photovoltaic array and pem electrolyser in solar-hydrogen systems for remote area power supply. In A thesis submitted in fulfillment of the requirements for the degree of Doctor of Philosophy. RMIT University.
- Pepijn (2020). Webinar on pv module quality and testing. https://www.linkedin.com/posts/pepijnveling_new-pv-module-solar-panel-types-are-flooding-activity-6694157303244959744-S-e6. Accessed: 07-08-2020.
- Peters, D. I. R. (2020). World first: An offshore pilot plant for green hydrogen. <https://bit.ly/3fgHgrk>. Accessed: 09-07-2020.
- Pó, M., Hoogendijk, K., Chiba, I., Akiyama, A., and Beuttell, W. (2018). Direct normal irradiance measurements using a tracker-less sunshine duration measurement concept. Accessed: 05-08-2020.
- PVEDucation (2019). Nominal operating cell temperature. <https://www.pveducation.org/pvcdrom/modules-and-arrays/nominal-operating-cell-temperature>. Accessed: 04-08-2020.
- Rahim, A. A., Tijani, A. S., Fadhlullah, M., Hanapi, S., and Sainan, K. (2015). Optimization

- of direct coupling solar pv panel and advanced alkaline electrolyzer system. *Energy Procedia*, 79:204–211.
- Regine Reissner, Jan Vaes, S. S. H. (2015). Review of electrolyser system with special emphasis on the hysolar system. In *RESElyser: System Concept for a combined RES-Electrolyser plant with optimised efficiency*. Project RESElyser.
- Ridley, B., Boland, J., and Lauret, P. (2010). Modelling of diffuse solar fraction with multiple predictors. *Renewable Energy*, 35(2):478–483.
- Rosa-Clot, M. and Tina, G. M. (2017). *Submerged and Floating Photovoltaic Systems: Modelling, Design and Case Studies*. Academic Press.
- Saadsaoud, M., Ahmed, A., Er, Z., and Rouabah, Z. (2017). Experimental study of degradation modes and their effects on reliability of photovoltaic modules after 12 years of field operation in the steppe region. *Acta Physica Polonica A*, 132(3):930–935.
- Sandia National Laboratories (2018). Pv performance modeling collaborative | single diode equivalent circuit models. <https://pvpmc.sandia.gov/modeling-steps/2-dc-module-iv/diode-equivalent-circuit-models/>. (Accessed on 08/09/2020).
- Sayedine, F., Maroufmashat, A., Sattari, S., Elkamel, A., and Fowler, M. (2016). Optimization of photovoltaic electrolyzer hybrid systems; taking into account the effect of climate conditions. *Energy conversion and management*, 118:438–449.
- Schröder, V., Emonts, B., Janßen, H., and Schulze, H.-P. (2004). Explosion limits of hydrogen/oxygen mixtures at initial pressures up to 200 bar. *Chemical Engineering & Technology: Industrial Chemistry-Plant Equipment-Process Engineering-Biotechnology*, 27(8):847–851.
- Schucan, T. (2000). International energy agency hydrogen implementing agreement final report for subtask a of task 11 – integrated systems. <https://bit.ly/3iBnmIP>. Accessed: 2020-6-18.
- SOLARGIS, W.-B. (2020). Global solar atlas. <https://globalsolaratlas.info/map?c=17.308688,7.03125,2&m=site>. Accessed: 24-07-2020.
- Stellbogen, D., Mohring, H., Jagomägi, A., Möttus, E., Friesen, G., Domine, D., Fabero, F., Betts, T., Gottschalg, R., Zdanowicz, T., et al. (2010). Comparative outdoor characterisation of pv modules across europe. In *Proceedings of the 25th Photovoltaic Solar Energy Conference, WIP, Valencia*, pages 3774–3778.
- Szyszkla, A. (1998). Ten years of solar hydrogen demonstration project at neunburg vorm wald, germany. *International Journal of Hydrogen Energy*, 23(10):849–860.
- Ulleberg, Ø. (2003). Modeling of advanced alkaline electrolyzers: a system simulation approach. *International journal of hydrogen energy*, 28(1):21–33.
- Ursúa, A., Barrios, E. L., Pascual, J., San Martín, I., and Sanchis, P. (2016). Integration of commercial alkaline water electrolyzers with renewable energies: Limitations and improvements. *International Journal of Hydrogen Energy*, 41(30):12852–12861.
- van Kruijsdijk, C. (2020). Skype conversation with dr. cor van kruijsdijk, sr. principal physicist, shell, amsterdam.
- Yakdehige, S. K. D. S. (2017). Design of an alkaline electrolysis stack. Master’s thesis, Universitetet i Agder; University of Agder.

A

Appendix

A.1. PV module characteristic



ELECTRICAL DATA | STC*

CS6K	300MS
Nominal Max. Power (Pmax)	300 W
Opt. Operating Voltage (Vmp)	32.5 V
Opt. Operating Current (Imp)	9.24 A
Open Circuit Voltage (Voc)	39.7 V
Short Circuit Current (Isc)	9.83 A
Module Efficiency	18.33 %
Operating Temperature	-40°C ~ +85°C
Max. System Voltage	1000 V (IEC) or 1000 V (UL)
Module Fire Performance	TYPE 1 (UL 1703) or CLASS C (IEC 61730)
Max. Series Fuse Rating	15 A
Application Classification	Class A
Power Tolerance	0 ~ + 5 W

* Under Standard Test Conditions (STC) of irradiance of 1000 W/m², spectrum AM 1.5 and cell temperature of 25°C.

Figure A.1: Electrical Data of Module

MECHANICAL DATA

Specification	Data
Cell Type	Mono-crystalline, 6 inch
Cell Arrangement	60 (6×10)
Dimensions	1650×992×40 mm (65.0×39.1×1.57 in)
Weight	18.2 kg (40.1 lbs)
Front Cover	3.2 mm tempered glass
Frame Material	Anodized aluminium alloy
J-Box	IP67, 3 diodes
Cable	4 mm ² (IEC) or 4 mm ² & 12 AWG 1000 V (UL), 1000 mm (39.4 in)
Connector	T4 (IEC/UL)
Per Pallet	26 pieces, 520 kg (1146.4 lbs)
Per container (40' HQ)	728 pieces

TEMPERATURE CHARACTERISTICS

Specification	Data
Temperature Coefficient (Pmax)	-0.39 % / °C
Temperature Coefficient (Voc)	-0.30 % / °C
Temperature Coefficient (Isc)	0.053 % / °C
Nominal Operating Cell Temperature	45±2 °C

Figure A.2: Mechanical data and Temperature Characteristics

Figure A.1 and A.2 gives the detailed description for the module used in the Setup.

A.2. Electrolyzer characteristics

MODEL	HySTAT-10-10	
Operating Pressure	10 barg	
Nominal hydrogen flow	10 Nm ³ /h	
Nr. of cell stacks	1	
Hydrogen flow range	40 - 100% (25 - 100% as an option)	
Hydrogen Purity (before HPS)*	99,9%; H ₂ O saturated, O ₂ < 1,000 ppm	
Hydrogen Purity (after HPS)	99,998% (99,999% as an option); O ₂ < 2ppm; N ₂ < 12ppm; Atm. Dew point: -60°C or -76°F (-75°C or -103°F as an option)	
Estimated AC power consumption (all included)	5,4 kWh/Nm ³ at full capacity	
Voltage	3 x 400 VAC ± 3% (3 x 480 or 575 VAC ± 3% as an option)	
Frequency	50 Hz ± 3% / 60 Hz ± 3% (option)	
Installed power	100 + 35KVA	
Max. cooling water temperature (electrolyte)	Closed loop cooling circuit installed	
Design flow cooling water (electrolyte)		
Max. cooling water temperature (gas cooling)	Chiller gas cooling circuit installed	
Design flow cooling water (gas cooling)		
Deminerzalized water consumption	Feed water purification system installed	
Tap water consumption	1,5 - 2 liters/Nm ³ H ₂	
Electrolyte	H ₂ O + 30% wt. KOH	
Electrolyte Quantity	220 L	
Installation area	Outdoor, general purpose area (optional indoor)	
Ambient Temperature Range	-20°C to +40°C (-40°C or +50°C as an option)	
Dimensions (L X W X H)	6,10m x 2,44m x 2,90m (+1,60m with dry cooler)	
Empty weight	Approx. 16 Tons	

Figure A.3: Electrolyzer datasheet

A.3. Inverter characteristics

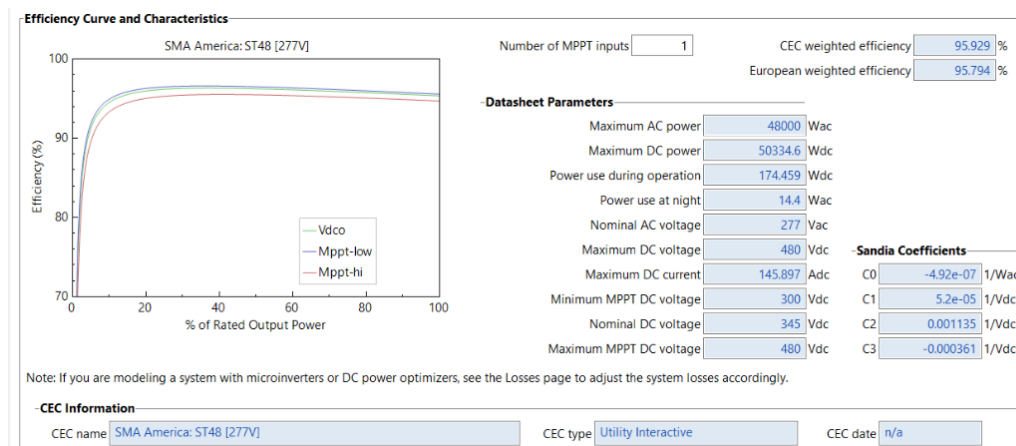


Figure A.4: Coefficients of CEC model for Inverter